AFIT/GM/ENP/98M-03

REGRESSION ANALYSIS OF RADAR MEASURED
OPTICAL TURBULENCE WITH SYNOPTIC SCALE
METEOROLOGICAL VARIABLES

THESIS

Diana L. Hajek, Captain, USAF

AFIT/GM/ENP/98M-03

Approved for public release; distribution unlimited

19980409035

AFIT/GM/ENP/98M-03

AFIT/GM/ENP/98M-03

REGRESSION ANALYSIS OF RADAR MEASURED OPTICAL TURBULENCE
WITH SYNOPTIC SCALE METEOROLOGICAL VARIABLES

THESIS

Presented to the Faculty of the Graduate School of Engineering

of the Air Force Institute of Technology

Air University

Air Education and Training Command

In Partial Fulfillment of the Requirements for the

Degree of Master of Science in Meteorology

Diana L. Hajek
Captain, USAF

March 1998

Approved for public release; distribution unlimited

AFIT/GM/ENP/98M-03

REGRESSION ANALYSIS OF RADAR MEASURED OPTICAL TURBULENCE
WITH SYNOPTIC SCALE METEOROLOGICAL VARIABLES

Diana L. Hajek, B.S.
Captain, USAF

Approved:

Cecilia A. Askue

Lt Col Cecilia A. Askue
Chairman, Advisory Committee

3 March 1998
Date

Mud KWalts

Lt Col Michael K. Walters
Member, Advisory Committee

6 MAR 98
Date

Won B. Roh

Dr. Won B. Roh
Member, Advisory Committee

6 Mar 98
Date

Daniel E. Reynolds

Prof. Daniel E. Reynolds
Member, Advisory Committee

3 March 1998
Date

Acknowledgments

I would like to thank my thesis advisor, Lieutenant Colonel Cecilia A. Askue, and my committee members, Lieutenant Colonel Michael K. Walters, Dr. Won B. Roh and Professor Daniel E. Reynolds for their advice and support throughout the course of this thesis effort. I'd also like to express my appreciation to the thesis sponsor, Air Force Research Laboratory, especially Major Michael Johnson, Captain Robert Asbury and Dr. Frank Eaton. Their guidance and support enabled the completion of this research project.

I'd also like to express my appreciation to Major Cliff Dungey who helped with understanding physical processes related to optical turbulence. Special thanks goes to our weather laboratory technician, Master Sergeant Pete Rahe. His help in understanding how to manipulate files in the Unix environment while providing needed space for new data was a lifesaver.

Most importantly, I'd like to express my gratitude to my husband whose patience and understanding have allowed me to focus on this project and my entire master's degree program. His support and motivation was invaluable to me over the past twenty-two months of this program.

Table of Contents

List of Figures

List of Tables

AFIT/GM/ENP/98M-03

Abstract

A key issue to the U. S. Air Force's Airborne Laser (ABL) program is the ability to accurately predict the level of optical turbulence that the ABL will encounter at flight levels in the upper troposphere and lower stratosphere. The optical turbulence must be characterized so that the range and range variation of the ABL can be determined. Gravity wave spectra resulting from frontal or jet stream passage are presumed to cause layers of optical turbulence; however, exact relationships between optical turbulence and synoptic scale meteorological phenomena are unclear.

This study assesses the statistical relationship between optical turbulence and synoptic scale variables through multiple linear regression. The optical turbulence measurements were measured by the 50 MHz radar at White Sands Missile Range, New Mexico from the discontinuous period between January 1993 to January 1994. Measurements were averaged temporally and vertically to coincide with weather data. The synoptic scale meteorological data was extracted from the National Center for Environmental Prediction/National Center for Atmospheric Research reanalysis database.

Results from the regression models showed that a linear relationship exists between the logarithm of optical turbulence and major synoptic scale variables; however, this relationship was a weak one. Based on this, it was concluded that further research was needed to define the exact relationship between synoptic scale meteorological variables and optical turbulence.

REGRESSION ANALYSIS OF RADAR MEASURED OPTICAL TURBULENCE WITH SYNOPTIC SCALE METEOROLOGICAL VARIABLES

1. Introduction

1.1 Background

Operation Desert Storm showed that U. S. armed forces have limited capability against theater ballistic missiles. The U.S. military's current defense are weapons such as the Patriot which destroy missiles near the end of their trajectory. There is no capability to defend against missiles shortly after they have been launched--also known as the boost phase. To fulfill this need, the U. S. Air Force developed the Airborne Laser (ABL) program. This program will involve placing a multimegawatt laser, a beam control system, and related equipment on a Boeing 747-400 aircraft, enabling detection and destruction of enemy missiles during their powered boost phase of flight (GAO, 1997:1).

The concept of the ABL system is to detect an enemy missile shortly after its takeoff, track the missile's path, and direct a concentrated laser beam on the missile until the beam's heat causes the missile's pressurized casing to fracture and explode igniting the remaining fuel. This explosion would cause the missile's warhead, in addition to any nuclear, chemical or biological agents it may carry, to fall short of its intended target (GAO, 1997:2). The window of opportunity is only from the time the missile clears the cloud tops to its booster burnout, since the missile is under pressure only while burning. The window can range from 30 to 140 seconds based on missile type. ABL's concept is shown in Figure 1.

Altitude (feet)

Window of opportunity
30 to 140 seconds

120,000

Booster burnout

100,000

80,000   Missile
                destroyed
                                                Destruction
                    Laser Dwell
60,000
                                                Tracking

40,000

                                                Detection
        ⌂ ᐃᗢᐃ Cloud Tops ᐃᗢᐃ ᐃᗢᐃ
20,000
        ⌂ ᐃᗢᐃ ⌂ ᐃᗢᐃ ᐃ ᐃᗢᐃ

        ⌂ ᐃᗢᐃ ⌂ ᐃᗢᐃ ᐃ ᐃᗢᐃ
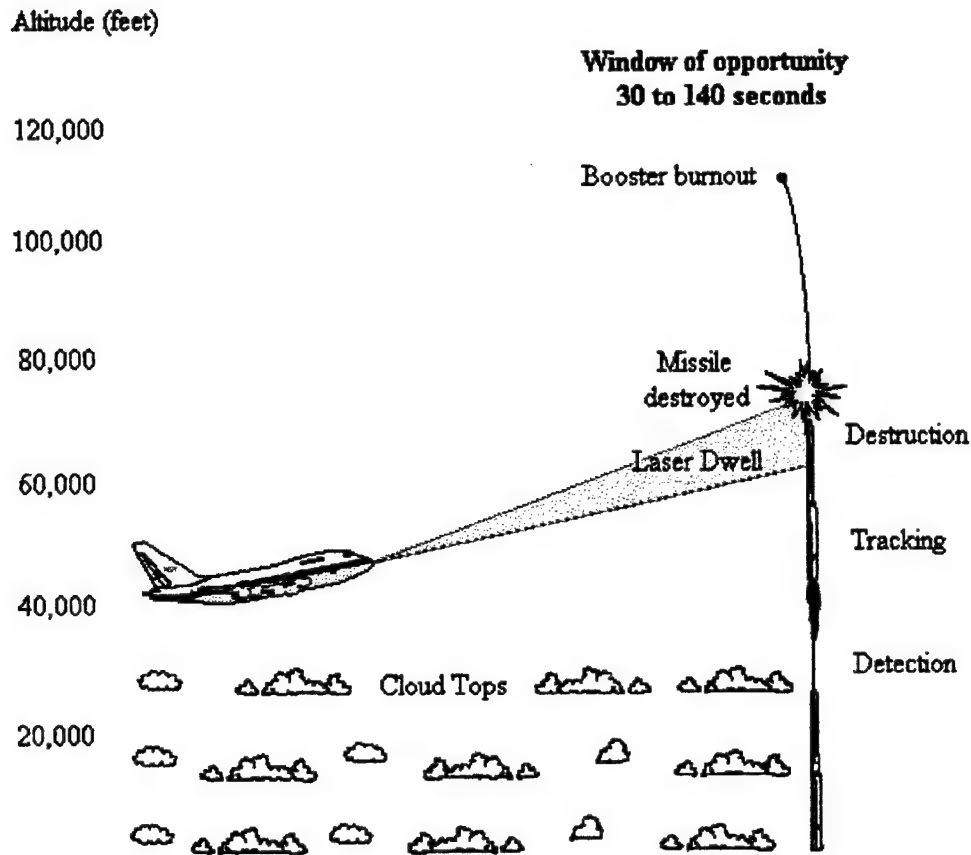
Figure 1. ABL Concept (GAO, 1997:5)

1.2 Significance of the Problem

A key issue to ABL's success is the ability to predict the level of optical turbulence that

the ABL is expected to encounter at flight levels in the upper troposphere and lower

stratosphere (GAO, 1997:2). This atmospheric optical turbulence must be characterized

so the range and range variation for the ABL can be established. Optical turbulence, also

known as the refractive index structure parameter, is the single most important factor in

determining the electromagnetic wave propagation characteristics in the troposphere and

stratosphere (Warnock and VanZandt, 1985:1). The ABL, therefore, must be able to

compensate for the optical turbulence in order to maximize its range and decrease its range variation.

Gravity wave spectra resulting from activity such as frontal passage or jet stream passage are presumed to cause layers of optical turbulence (Nastrom and Eaton, 1993a:1; Bluestein, 1993:568). However, exact relationships between optical turbulence and synoptic scale meteorological phenomena are unclear, and continuous sets of optical turbulence measurements for extended periods of time are rare (Nastrom and Eaton, 1993b:1). If a strong statistical relationship between optical turbulence and major synoptic features can be found, a means of forecasting optical turbulence through synoptic scale variables can be established. This statistical relationship is related to the range and range variation of ABL technology which will be addressed in the program's Authority to Proceed milestone scheduled for summer 1998.

1.3 Problem Statement

What statistical relationship exists between radar measured values of optical turbulence and major synoptic scale meteorological variables?

1.4 Benefit from Solving the Problem

A strong statistical relationship between optical turbulence, characterized by the refractivity structure parameter C_n^2, and specific synoptic features would enable the ABL team to establish trends of C_n^2 anywhere on the globe deriving them from archived synoptic scale climatology. A strong relationship would also provide the ABL team with a guide as to where to collect C_n^2 data. As mentioned in 1.2, the ability to forecast C_n^2 plays

3

a major role in demonstrating the ABL's range and range variation. Weak correlation between C_n^2 and synoptic variables would still provide useful information to the ABL team--it would eliminate one method of forecasting optical turbulence. In this case, the ABL team may explore other C_n^2 forecasting methods, possibly based on local or mesoscale phenomena, in order to demonstrate the range of the ABL.

1.5 Scope

This study was focused on determining what statistical relationship existed between optical turbulence measurements taken from the 50 Megahertz (MHz) radar at White Sands Missile Range, New Mexico, and corresponding synoptic scale meteorological variables extracted from the National Center for Environmental Prediction/National Center for Atmospheric Research (NCEP/NCAR) reanalysis database through multiple linear regression. Specifically, this study determined the relationship between C_n^2 and variables associated with fronts, jet streams, the Bulk Richardson Number and the ageostrophic wind at the synoptic scale. Details on the data set will be discussed in Chapter 4.

This study did not specifically correlate turbulence to gravity wave activity using indicators such as the variance of vertical velocity (Nastrom and Eaton, 1993b:82). However, since some non-convective gravity waves can be generated by frontogenetical processes or by air parcels moving through jet streaks, gravity wave activity was accounted for in this study (Bluestein, 1993:568). For example, the maximum zonal and meridional winds were included as potential predictors in the regression models. Gravity waves may be related to these winds; therefore, gravity wave activity was indirectly accounted for.

4

1.6 General Approach

This research consisted of two main parts: data processing and multiple regression analysis as described below.

1.6.1 Data Processing.

The radar measured C_n^2 data and the climatological data from the NCEP/NCAR reanalysis database was provided by the thesis sponsor, Air Force Research Laboratory (AFRL). Meteorological parameters associated with fronts, jet streams and the bulk Richardson Number were extracted from the NCEP/NCAR reanalysis database to correspond to the location and dates for which C_n^2 data was collected. Since the climatological and C_n^2 data was not simultaneous, the C_n^2 values were averaged in six hour increments to coincide with the weather data. The turbulence measurements were also averaged vertically in 300 meter increments at altitudes corresponding to tropopause heights.

1.6.2 Multiple Regression Analysis.

Multiple regression analysis was performed with the C_n^2 value at varying altitudes as the dependent variable and the meteorological values as the independent variables. Multiple regression analysis was appropriate because it measured the degree of association between the turbulence and synoptic scale meteorological values (Tabachnick and Fidell, 1983:86). The SAS computer statistics package was used to complete the regression analysis.

1.7 Thesis Organization

Chapter 2 discusses past and recent literature related to the problem under investigation. It describes methods used to gain an understanding of small scale

5

turbulence by studying C_n^2 using measurements from wind profiler radars. It also describes some modeling efforts and their comparisons to wind profilers. Finally, it provides a synopsis of results expected based on the literature search.

Chapter 3 provides an overview of the theory of optical turbulence and how it relates to radar. It also provides details on the radar at White Sands Missile Range, New Mexico used to make the C_n^2 measurements. Lastly, it describes the data processing method which includes an outline of the theory behind some of the meteorological variables derived.

Chapter 4 describes the NCEP/NCAR reanalysis database and the meteorological data extracted from it and the C_n^2 data observed using the White Sands Missile Range radar. It also explains the statistical tools employed in the data analysis such as multiple linear regression.

Finally, Chapter 5 presents the results and conclusions of this study. Recommendations for further research are also given.

2. Literature Review

2.1 Early Work

Understanding small scale turbulence enables us to understand the general circulation of the atmosphere including effects on propagation of electromagnetic waves (Nastrom and others, 1986:6722; Nastrom and Eaton, 1993b:81). One method to gain an understanding of turbulence is to study its parameters, such as the refractivity turbulence structure parameter, C_n^2. The ability to measure turbulence parameters was enhanced in the 1970s and 1980s with use of pulsed radars, called wind profilers, capable of detecting returns from the clear air. Measurements by balloon, aircraft or optical techniques were also available, but usually limited to short campaigns (Nastrom and others, 1986:6722). Finally, modeling also played a major role in estimating turbulence parameters in the late 1970s and 1980s.

2.1.1 VanZandt and others, 1978.

In their research, VanZandt and others compared observations of C_n^2 measured by a Doppler radar with results from a theoretical model. The hypothesis of their paper was to determine if fluctuations in refractive index measured by radar were close to values of optical turbulence calculated by their model. The model they developed calculated C_n^2 from rawinsonde profiles of wind, temperature and humidity. The radar observations were measured by Doppler radar which is located about 15 kilometers west of Boulder, Colorado (VanZandt and others, 1978: 819).

7

First, VanZandt and others described their radar measured optical turbulence values. Measurements were taken every 50 seconds at heights ranging from 5 to 15 kilometers. Since the C_n^2 observations varied rapidly with time, they averaged their 50-second measurements to 22 to 72-minute averages (VanZandt and others, 1978:822). They then compared C_n^2 measurements for 8 March 1978, which had light winds, and 19 March 1978, which had a moderate jet stream. Their results indicated that the magnitude of C_n^2 increased with increasing vertical shear (VanZandt and others, 1978:823).

Next, they discussed the model calculations and compared both sets of data for five different days. There was a basic agreement between the model and radar observations so their calculations strongly supported their hypothesis. Their comparison also indicated relative maxima in C_n^2 magnitude in regions of maximum shear above and below the peak of the jet stream in both the radar and model values (VanZandt and others, 1978:827).

The good agreement between radar observations and model calculations denoted that both the radar reflectivity and theoretical model were good estimators of the vertical profile of optical turbulence. Therefore, since radars have both excellent temporal and spatial resolution, measurements will be extremely useful for studying time and space variations of C_n^2 (VanZandt and others, 1978:827).

2.1.2 Warnock and VanZandt, 1985.

Warnock and VanZandt described and provided computer code for a modified version of the statistical model described in 2.1.1. This version of the model estimated average values of C_n^2 for layers of atmosphere about 150 meters thick from National Weather Service balloon data or a comparable data set. The use of a statistical model was

8

appropriate because they believed that the random fluctuations of refractive index and other related physical characteristics were best described by statistics. They further supported their use of a statistical model by stating that direct calculation of C_n^2 required precise measurements of the meteorological values and their gradients with a spatial resolution of approximately one meter throughout the entire atmosphere. Since this data was not available, they relied on measurable large-scale quantities and statistics (Warnock and VanZandt, 1985:2).

They also explained that fine-scale turbulent flows are embedded in the large-scale laminar flow in thin, stratified layers. They suggested these local turbulent flows were caused by shear instability in areas where the large-scale flow is stable, but where the fine-scale flow is unstable (Warnock and VanZandt, 1985:3). They also described thinner layers, several tens of meters or thinner, occurring more often, with many in the troposphere and stratosphere at any time (Warnock and VanZandt, 1985:4).

2.1.3 Warnock and others, 1985.

Warnock and others compared 12 winter and 22 summer profiles of radar-measured and model-calculated values of C_n^2 from the revised model just described in 2.1.2. For each season, large variations in C_n^2 were encountered, sometimes near two orders of magnitude or greater at one specific height.

Warnock and others found the model's calculations agreed with the radar data. More importantly, the model's calculations provided insight into what weather conditions caused the C_n^2 fluctuations. During the winter period, they discovered that large increases in wind shear accompanying jet-stream passages increased the intensity of turbulence and thus

9

produced large increases in C_n^2. During the summer, without strong convection, C_n^2 values above 10 kilometers were similar to winter values; however, below 10 kilometers the summer values were greater than winter values even under light wind conditions. Warnock and others showed that these greater C_n^2 values were due to the humidity and humidity gradients contributing to the refractive index and were not caused by increased turbulence intensity (Warnock and others, 1985:158).

2.1.4 Nastrom and others, 1986.

Nastrom and others studied the variability of C_n^2 at altitudes of 4 to 20 kilometers measured by the Doppler radars at Poker Flat, Alaska, and Platteville, Colorado (Nastrom and others, 1986:6722). The data from the Poker Flat radar was taken from September 1981 to September 1982. Observations from the Platteville radar were taken from April 1983 to February 1984 (Nastrom and others, 1986:6724). They investigated variations of C_n^2 over 30 day periods by examining 3-hour medians. Medians were used instead of means because they were less sensitive to extreme values due to interference such as reflections from airplanes (Nastrom and others, 1986:6725).

They found that C_n^2 followed a lognormal distribution at all heights they sampled. This enabled them to statistically analyze the data assuming a normal distribution.

They first calculated the autocorrelation function for all 9-hour intervals where at least 85% of the observations remained after data editing was completed. The individual functions were then averaged and examined (Nastrom and others, 1986:6727). They determined that the autocorrelation function could be modeled as the sum of a random process and first order autoregressive process (Nastrom and others, 1986:6733). Since

10

the autocorrelation function also estimates the effective time between independent values of C_n^2, they found the effective time decreased with height from 25 to 45 minutes in the troposphere to approximately 18 minutes in the stratosphere. In other words, in the stratosphere, a C_n^2 value is no longer related to the C_n^2 value measured 18 minutes after it (the autocorrelation function is described further in 4.2.1). They also noted that the logarithm of C_n^2, abbreviated as log (C_n^2), had the largest mean value when the autocorrelation value was the largest (Nastrom and others, 1986:6728).

Second, they computed monthly averages of the 3 hour medians, or monthly means of the medians, of log (C_n^2) (Nastrom and others, 1986:6730). The data showed largest monthly means in the winter with a secondary maximum in the summer. The winter maximum is related to enhanced baroclinic activity such as wind speed, wind shear and gravity waves. The summer maximum is related to increased convection (Nastrom and others, 1986:6733).

Finally, they examined the relationship between C_n^2 and other variables using correlation coefficients. The coefficients indicated that log (C_n^2) at every level was most closely correlated with wind speed near the tropopause. They also found that conditions near the surface seemed to affect C_n^2. Nastrom and others stated that in specific cases, C_n^2 relied on the synoptic weather picture and not just the wind flow and static stability where the turbulence was measured. Furthermore, a strong correlation between C_n^2, gravity waves and background wind was discovered (Nastrom and others, 1986:6731).

2.1.5   Tsuda and others, 1988.

Tsuda and others discussed echoes observed in the troposphere and lower stratosphere in September 1986 by the middle and upper (MU) radar site in northern Japan. They also touched upon mechanisms that determine refractive index gradients in the atmosphere above 10 kilometers or what they referred to as the dry atmosphere. Finally, they discussed effects of gravity waves on layers in the dry atmosphere (Tsuda and others, 1988:655).

Data was collected at vertical heights ranging from about 5 kilometers to 21 kilometers with a vertical resolution of 150 meters and temporal resolution of 74 seconds. The data was then averaged over five records to condense the data set. After examining the data, they found a thin, concentrated, echoing layer between 9-12 kilometers and moderately stratified reflection layers with upward and downward phase progressions in the stratosphere (Tsuda and others, 1988:656). They suggested this intense layer between 9 and12 kilometers corresponded to a region of large vertical shear, characterizing large temperature gradients in both the vertical and horizontal directions. Weaker layers observed in the troposphere were also related to areas of strong wind shear (Tsuda and others, 1988:659). Finally, they suggested gravity waves affected the reflection layers, causing temperature fluctuations in the stratosphere (Tsuda and others, 1988:656-658).

2.2 Recent Work

Recent studies of optical turbulence have shifted from wind profiler radars to radars with better resolution. In the past few years, scientists have taken advantage of very high frequency (VHF) Doppler radars that provide excellent spatial and temporal resolution for

12

measuring C_n^2. They also provide the capability to obtain C_n^2 data sets with observations taken on a continuous basis for extended periods of time.

2.2.1 Frisch and others, 1990.

Frisch and others calculated monthly mean backscattered power for five years using observations from the 50-megahertz (MHz) wind profiler in Fleming, Colorado. Their purpose in this study was to better understand variations in the backscattered signals and C_n^2, since backscattered power is directly proportional to C_n^2. They suggested that understanding these variations would provide further insight into atmospheric turbulent processes (Frisch and others, 1990:645-646).

Frisch and others averaged the backscattered power into 2-kilometer intervals and then over a thirty-day period (Frisch and others, 1990:647). After reviewing the data, they discovered changes of 2 decibels (dB) or larger in the year-to-year variation of C_n^2 (Frisch and others, 1990:651). They also found a seasonal cycle in C_n^2 below the tropopause in addition to the year-to-year change. In contrast, they found no seasonal variation above the tropopause. They also studied a record of backscattered power from the Stapleton aiport wind profiler in Denver, Colorado, and found comparable longer-term trends (Frisch and others, 1990:645).

2.2.2 Nastrom and Eaton, January 1993.

Nastrom and Eaton studied the winds and turbulence using observations from the 50-megahertz (MHz) VHF Doppler radar at White Sands Missile Range (WSMR), New Mexico. They demonstrated that under specific conditions, C_n^2 values in the lower

stratosphere vary by up to an order of magnitude depending on the source of gravity wave activity in the lower atmosphere (Nastrom and Eaton, 1993b:81).

Observations were obtained for 10 days in March and April 1991, providing a continuous data set. Inherent in the observations was a variety of synoptic weather patterns such as surface cold fronts, surface troughs and ridge axes. Data was available in 3-minute increments at 150-meter resolution for altitudes from about 3 to 20 kilometers (Nastrom and Eaton, 1993b:82).

Nastrom and Eaton compared mean values of the logarithm of C_n^2 to high and low wind speeds at 5.6 kilometers (Nastrom and Eaton, 1993b:84). The wind speed at 5.6 kilometers was used as an indicator of synoptic weather activity (Nastrom and Eaton, 1993b:86). They showed that mean values of the logarithm of C_n^2 were greater at all heights during periods of strong winds than during periods of weak winds. The increased values of C_n^2 in the lower troposphere were probably due to enhanced moisture present during passage of fronts and troughs that were connected dynamically with the strong winds at 5.6 kilometers. Larger values of C_n^2 at higher altitudes were probably due to increases in turbulence (Nastrom and Eaton, 1993b:84).

Nastrom and Eaton hypothesized that enhanced turbulence in the stratosphere during periods of high winds at 5.6 kilometers was due to the breaking of upward-propagating gravity waves that were generated by conditions in the lower troposphere related to troughs (Nastrom and Eaton, 1993b:86). They concluded that that future models of C_n^2 should account for the intensity of gravity-wave source mechanisms in addition to

14

variables related to the background flow such as mean wind and temperature (Nastrom and Eaton, 1993b:87).

2.2.3 Nastrom and Eaton, 1995.

Nastrom and Eaton (1995) described the average vertical profiles of winds and turbulence and their seasonal and diurnal changes using data measured by WSMR radar (Nastrom and Eaton, 1995:2135). The general time period for observations taken for their study was from January 1991 to April 1994 (Nastrom and Eaton, 1995:2137).

First, Nastrom and Eaton found the measurements of the logarithm of C_n^2 to be normally distributed (Nastrom and Eaton, 1995:2141). Second, their data showed that the largest values of C_n^2 in the troposphere were found in the summer and were related to areas of high humidity. In spring, fall and winter and in the stratosphere, there was little variation in C_n^2. This probably occurred because the mean wind shear was fairly constant with season, and the mean static stability in the stratosphere changed little with season (Nastrom and Eaton, 1995:2143). Finally, they noticed relatively small diurnal variations in the logarithm of C_n^2 (Nastrom and Eaton, 1995:2145). The largest diurnal variation they did find, however, was in the troposphere during summer and had a range of about 5 decibels (Nastrom and Eaton, 1995:2147).

2.3 Results Expected

Based on the literature summarized above, it seemed reasonable to average C_n^2 data temporally and spatially for this study's requirements, and to define the relationship

15

between C_n^2 and weather variables statistically. In addition, a strong statistical relationship between the logarithm of C_n^2 and the following variables was expected:

(1) Near-tropopause wind

(2) Ageostrophic wind

(3) Bulk Richardson number (which is inversely proportional to wind shear assuming constant static stability)

3. Methodology

3.1 Theory

The index of refraction of the atmosphere for electromagnetic waves depends on the temperature and humidity of the air (Tatarski, 1961:1). The potential refractivity, derived below, can be used to calculate the size of fluctuations in the refractive index caused by temperature and humidity changes (Tatarski, 1961:58). The structure function, which characterizes the intensity of refractive index fluctuations, and its associated structure parameter is also given (Tatarski, 1961:10). Lastly, the relationship between the refractivity structure parameter, received power and radar reflectivity is provided.

3.1.1 Index of Refraction.

The index of refraction n for radio waves is a function of temperature T (K), pressure p (mb), and vapor pressure e (mb) (Tatarski, 1961:55). This relationship can be shown as:

$$n - 1 = 10^{-6} \frac{79}{T} \left(p + \frac{4800e}{T} \right). \qquad (1)$$

Any rapid change in the pressure, temperature or humidity can cause rapid changes in the refractive index. Since rapid changes in pressure over very small distances are highly unlikely, fluctuations in the index of refraction are mostly caused by large temperature and humidity irregularities in the air (Rinehart, 1991:148).

Some properties of the atmosphere can be regarded as conservative quantities or quantities that remain constant during certain transformations (Tatarski, 1961:40;

17

Wallace and Hobbs, 1977:69). The variables T and e in (1) are not conservative; therefore, they may affect the dynamics of the turbulence (Tatarski, 1961:40,55). For example, when small parcels of air are moved vertically, their pressure undergoes a continuous equalization process with the ambient pressure at each altitude.

These pressure changes create temperature changes which satisfy the following equation:

$$\frac{dT}{T} = \frac{\gamma - 1}{\gamma} \frac{dp}{p},\qquad(2)$$

where

$\gamma = c_p / c_v$

c_p = specific heat at constant pressure ($J\,K^{-1}\,kg^{-1}$)

c_v = specific heat at constant volume ($J\,K^{-1}\,kg^{-1}$).

The quantity dp in (2) is related to the change in height dz (m) by the hydrostatic approximation:

$$\frac{dp}{dz} = -\rho g,\qquad(3)$$

where ρ is the density of the air (kg/m^3) and g is the acceleration due to gravity (9.8 m/sec^2). Using the ideal gas law, one can show that:

$$\frac{dT}{T} = -\frac{\gamma - 1}{\gamma} \frac{\rho g}{p} dz = -\frac{\gamma - 1}{\gamma} \frac{g}{R_d T} dz \qquad(4)$$

and

$$\frac{dT}{dz} = -\frac{\gamma - 1}{\gamma} \frac{g}{R_d} = -\frac{g}{c_p} = -\gamma_a,\qquad(5)$$

18

where R_d is the ideal gas constant for dry air (287 J K^{-1} kg^{-1}) and γ_a is the dry adiabatic lapse rate (K/km). Integrating (5) leaves $T + \gamma_a z = const$ and when parcels are displaced vertically, the expression:

$$\theta = T + \gamma_a z \qquad (6)$$

gives the potential temperature θ (K) which is a conservative quantity. The vapor pressure e can also be transformed into a conservative quantity by expressing it in terms of specific humidity q (Tatarski, 1961:56):

$$e = 1.62 \, p q . \qquad (7)$$

Substituting (6) and (7) into (1) gives an expression with conservative quantities of θ and q (Tatarski, 1961:57):

$$(n-1) \times 10^6 = \frac{79 p}{\theta - \gamma_a z}\left(1 + \frac{7800q}{\theta - \gamma_a z}\right) . \qquad (8)$$

This form of the refractive index, however, is not a "good passive tracer" (Hocking, 1985:1406). This can be explained by the following situation. Suppose an air parcel is displaced from level z_1 to a new level z_2. Suppose at level z_1, the parcel was in equilibrium with the environment and at this level there was a pressure p_1, potential temperature θ_1 and specific humidity q_1. Suppose at level z_2, the ambient pressure is p_2 and the environmental potential temperature and specific humidity are θ_2 and q_2, respectively. At level z_2, the potential temperature and specific humidity of the parcel can be represented as θ_1 and q_1, since these are conservative quantities. The pressure of the parcel, however, has changed to p_2 at level z_2. The change in refractive index between the parcel and environment at level z_2 can be shown as:

$$\Delta n = n_{parcel}(z_2, p_2, \theta_1, q_1) - n_{environment}(z_2, p_2, \theta_2, q_2) \qquad (9)$$

or

$$\Delta n = \left(\frac{\partial n}{\partial \theta} \frac{\partial \theta}{\partial z} + \frac{\partial n}{\partial q} \frac{\partial q}{\partial z} \right) \Delta z, \qquad (10)$$

where $\Delta z = z_2 - z_1$. Equation (10) is not just the difference in refractive index at levels z_1 and z_2, which would have been (Hocking, 1985:1407):

$$\Delta n = \left(\frac{\partial n}{\partial p} \frac{\partial p}{\partial z} + \frac{\partial n}{\partial \theta} \frac{\partial \theta}{\partial z} + \frac{\partial n}{\partial q} \frac{\partial q}{\partial z} \right) \Delta z. \qquad (11)$$

Therefore, fluctuations which arise are not proportional to the total gradient of n, shown in (11), but rather to (10). This actual change is refractive index is referred to as the potential refractivity M shown as (VanZandt and others, 1978:823; Hocking, 1985:1407; Nastrom and Eaton, 1993a:23236):

$$M = -77.6 \times 10^{-6} \frac{p}{T} \left(\frac{\partial \ln \theta}{\partial z} \right) H_1, \qquad (12)$$

where

$$H_1 = 1 + \frac{15500q}{T} \left(1 - \frac{1}{2} \frac{\partial \ln q / \partial z}{\partial \ln \theta / \partial z} \right).$$

The value q dominates in the lower troposphere, but is negligible in the stratosphere where the average value of $\partial \ln \theta / \partial z$ is large (VanZandt and others, 1978:823; Hocking, 1985:1407). Therefore, in the stratosphere where it is relatively dry, H_1 is approximately equal to one (Nastrom and Eaton, 1993a:23236).

3.1.2 Refractivity Turbulence Structure Function and Parameter.

The structure function is a fundamental characteristic of a stationary random process. Generally speaking, the value of the structure function describes the intensity of the optical turbulence fluctuations (Tatarski, 1961:10).

The structure function $D_n(r)$ of the atmospheric refractive index for the inertial range can be shown as (Tatarski, 1961:58):

$$D_n(r) = \begin{cases} C_n^2 \, r^{2/3} & \text{for } l_o \ll r \ll L \\ C_n^2 \, l_o^{2/3} \left(\dfrac{r}{l_o} \right)^2 & \text{for } r \ll l_o \end{cases} \qquad (13)$$

where

r = spatial separation (m)

C_n^2 = refractivity turbulence structure parameter ($m^{-2/3}$)

l_o = inner scale of turbulence (size of smallest eddies) (m)

L = outer scale of turbulence (size of largest eddies) (m).

The inertial range is where large eddies break up into smaller eddies, due to fluid dynamic instabilities, and these smaller eddies break down into even smaller ones. This cascade of energy from large scales to smaller scales continues until the scale becomes so minute that viscosity effects are introduced. At this point, the energy flows out of the cascade into the sink of molecular heat (Dewan, 1980:11). The inertial subrange falls between the inner scale l_o and outer scale L of turbulence.

The refractivity turbulence structure parameter C_n^2 for the inertial subrange can be defined as:

$$C_n^2 = a^2 \alpha` L^{4/3} M^2 \ , \qquad\qquad (14)$$

where a^2 is a universal constant taken to be 2.8 and $\alpha`$ is a ratio of eddy diffusivities which is close to 1 (VanZandt and others, 1978:823; Ottersen, 1969:1182). Equation (14) is valid for homogeneous, isotropic, steady state turbulence. Turbulence is homogeneous and isotropic when the structure function, $D_n\ (r)$, does not depend on direction or location of r. Steady state can be interpreted as the amount of energy that flows into the turbulence being the same amount of energy dissipated into heat (Dewan, 1980:11).

3.1.3 Refractivity Turbulence Structure Parameter and Radar Reflectivity.

A source of clear air return in the atmosphere is from refractive index perturbations. When the index of refraction changes considerably over scales which are small compared to the radar wavelength, the area containing these small scale fluctuations can return some of the incident power back toward the radar. If the radar is sensitive enough, this can cause a detectable echo to be displayed on the radar (Rinehart, 1991:147). This relationship between the backscattered power and C_n^2 can be examined by first looking at the radar equation.

The radar equation is given by (Frisch and others, 1990:645):

$$\overline{P}_R = \frac{c}{1024\,\pi^2\,\ln 2}\ P_t\,G^2\theta_r\,\phi_r\,\tau\,\lambda^2\,\frac{\eta}{Ran^2}\ , \qquad\qquad (15)$$

22

where

$\overline{P}_R$ = received power, averaged over several independent realizations (W)

c = speed of light (3 x 10^8 m/sec)

P_t = transmitted power (W)

G = on-axis gain of the antenna

θ_r, ϕ_r = half-power beamwidths of the antenna (rad)

τ = pulse duration (sec)

λ = radar wavelength (m)

η = radar reflectivity (m^{-1}) or radar cross-section per unit volume

Ran = range from radar (m).

Equation (15) shows that the received power $\overline{P}_R$, also referred to as the backscattered power, is proportional to the radar reflectivity η.

In clear air, the radar reflectivity can be related to refractive index fluctuations with spatial scales $\lambda/2$ through the structure function in (13) (Ottersen, 1969:1182; Frisch and others, 1990:645). If $\lambda/2$ falls within the inertial subrange of turbulence, then the radar reflectivity is directly proportional to C_n^2 as shown (Ottersen, 1969:1183; Hocking, 1985:1411):

$$\eta \approx 0.38 \, C_n^2 \lambda^{-1/3}. \qquad (16)$$

Substituting (16) into (15) and solving for C_n^2 gives the following (Nastrom and others, 1986:6724):

$$C_n^2 = K \frac{Ran^2}{P_t} \overline{P}_R, \qquad (17)$$

23

where

$$K \approx \frac{18435}{\lambda^{5/3}G^2\theta_r \, \phi_r \, \tau c}.$$

Thus, C_n^2 is directly proportional to the radar backscattered power as well.

3.2 Radar Used to Collect C_n^2 Data

The 50-megahertz (MHz) radar used to collect C_n^2 values for this study is located at the Atmospheric Profiler Research Facility (APRF) at White Sands Missile Range, New Mexico, 32°24'N, 106°21'W (Hines and others, 1996:11; Nastrom and Eaton, 1993b:82). The APRF complex is positioned on the floor of the Tularosa basin approximately 1220 meters above mean sea level and about 10 kilometers east of the San Andres, San Augustine and Organ Mountains (Hines and others, 1996:13).

The 50-MHz profiler, manufactured by Tycho Technology, Inc., contains three antenna beams. Each antenna beam takes about 1 minute to make a measurement, so a full cycle takes about 3 minutes (Hines and others, 1996:18). One radar beam is pointed toward the zenith, while the other two radar beams are pointed 15° from the zenith; one is pointed toward the south and the other is pointed toward the west. The antenna has a diameter about 150 meters and generates a one-way beamwidth of 2.9° (Hines and others, 1996:113).

The radar functions at a central frequency of 49.25 MHz and a transmitted peak power of 250 kilowatts (kW) (Hines and others, 1993:113-114). Received power observed for one minute along each of three beams is used to calculate a full C_n^2 profile every 3 minutes at a 150-meter resolution. In normal mode, 112 range gates are used to sample from

24

about 3 to 20 kilometers above ground level (Hines and others, 1993:113; Nastrom and

Eaton, 1993b:82).

The radar equation used to compute C_n^2 from this 50 MHz radar is (Hines and others, 1993:114):

$$C_n^2 = \frac{112.16\lambda^{1/3} Ran^2 P_R}{\delta P_t L_t A_{em}}, \qquad (18)$$

where

λ = radar wavelength (m)

Ran = range from radar (m)

P_R = received power (W)

δ = range resolution (m)

P_t = peak power at transmitter (W)

L_t = total receiver and transmission line loss and antenna efficiency

A_{em} = effective antenna area (m^2).

Comparisons between annual mean C_n^2 measurements made by the south and west beams of the radar showed differences of about 1 dB in the troposphere and 2 dB in the stratosphere. It was suggested that this difference may indicate anisotrophy in small-scale turbulence (Nastrom and Eaton, 1995: 2144). It was necessary to increase average C_n^2 values in the west beam to coincide with the average values in the south beam.

Manufacturer's tests of the 50-MHz wind profiler show that the accuracy of the C_n^2 measurements are within ± 1.5 dB. The antenna is calibrated to ± 0.5 dB, but the difference between the oblique beams must be included in this uncertainty (Hines and

others, 1996:114). The parameters of the WSMR 50-MHz radar used in this study are summarized in Table 1.

Table 1. Radar parameters used in this study (Nastrom and Eaton, 1993b:2136).

TRANSMITTER	
Central frequency	49.25 MHz
Wavelength	6 m
Output power	250 kW peak
Duty cycle	5%
Pulse width	8 μsec
Type	Combination solid state preamplifier and tube cavity amplifier, three stage
ANTENNA	
Number of beams	3
Physical aperture	15,600 m^2
Effective aperture	13,500 m^2
Pointing	Zenith and 15° to south and west
Type	Coaxial collinear phased array
One way beamwidth	2.9°
RECEIVER	
Type	Low noise superheterodyne
Bandwidth	Matched to transmitted pulse
Receiver noise figure	Less than 1 dB
PERFORMANCE	
Nominal lowest range gate	2 km above ground level
Range gate spacing	150 m
Time resolution	1 min per beam (3 min total)
Number of range gates	112
Calibrated C_n^2 range	10^{-20}-10^{-13} $m^{-2/3}$
Bandwidth	1 MHz
Power aperture product	1×10^8 W/m^2
Error in C_n^2 measurements	± 1.5 dB

3.3 Data Processing

Both the meteorological and optical turbulence data had to be processed in order to complete the multiple regression analysis. The procedures are described below.

3.3.1 Meteorological Data

The synoptic scale meteorological data was extracted from the NCEP/NCAR reanalysis database and was provided by the sponsor, AFRL, in a non-gridded binary format. Data was provided for latitudes between 10° and 65° N and for the entire longitude grid. Since the radar site is located at 32°24'N, 106°21'W, a smaller grid was extracted from this grid to coincide with the radar location. This grid encloses the area between 30°-35°N and 102°30'-110°W with the radar site centrally located as shown in Figure 2. The intention was to have an area large enough to capture portions of the jet stream near or above the radar site.

The variables used in this data set are shown in Table 2. The levels indicate the number of pressure levels that particular variable is available for, with a maximum number of 17 pressure levels that range from 1000 to 10 millibars. If the variable is only available at one vertical level, no level is given. Note that all these variables can be considered related to fronts, jet streams or both. Therefore, all variables provided by AFRL were used as potential independent variables in the regression analysis with the exception of surface geopotential height since it varied little with time or space.

The ageostrophic wind and bulk Richardson number were derived from the other variables in Table 2. The procedures for these calculations are explained below.
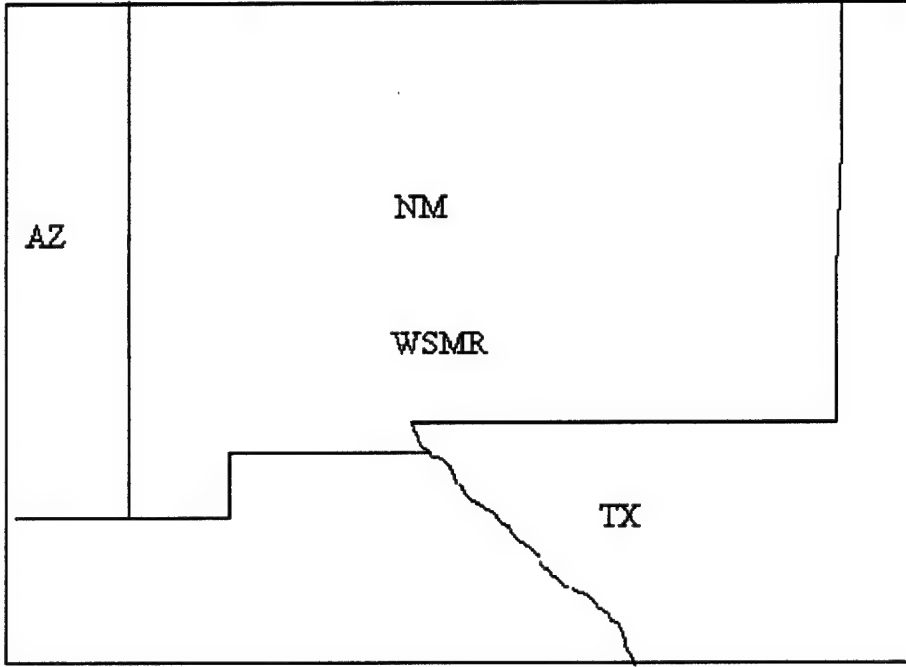
Figure 2. Grid used in this study. The 50 MHz radar is centrally located at WSMR.

3.3.1.1 Ageostrophic Wind.

An initial look at the relationship between the ageostrophic wind and C_n^2 by AFRL showed that a correlation may exist. The sponsor requested further investigation; therefore, the ageostrophic wind was included as another potential independent variable in the regression analysis.

The ageostrophic wind $\vec{V}_{ag}$ (where the arrow over V denotes a vector) was calculated using the difference between the total wind $\vec{V}$ and the geostrophic wind $\vec{V}_g$ or:

$$\vec{V}_{ag} = \vec{V} - \vec{V}_g.$$ (19)

The total wind components, U (east-west or zonal wind) and V (north-south or meridional wind), were given in the NCEP/NCAR data set; however, the geostrophic wind was

28

unknown. Since the geopotential height H was available, the geostrophic wind could be computed from the following cross product (Holton, 1992:59):

$$\vec{V}_g = \frac{1}{f} \hat{k} \times \nabla H, \qquad\qquad (20)$$

where f is the Coriolis parameter (sec^{-1}), $\hat{k}$ is the unit vector in the vertical direction, and ∇ is the gradient in rectangular coordinates.

Table 2. Meteorological variables used in this study.

VARIABLE	SYMBOL	LEVELS	UNITS
Surface pressure	PS		Pa
Temperature at tropopause	TT		K
Pressure at tropopause	PT		Pa
U-winds at tropopause	UT		m/sec
V-winds at tropopause	VT		m/sec
Wind shear at tropopause	SHT		1/sec
Surface lifted index	LI		K
Best (4-layer) index	B		K
Temperature at max wind level	TM		K
Pressure at max wind level	PM		Pa
U-winds at max wind level	UM		m/sec
V-winds at max wind level	VM		m/sec
Pressure reduced to mean sea level	PR		Pa
Geopotential height	H	17	m^2/sec^2
U-winds	U	17	m/sec
V-winds	V	17	m/sec
Ageostrophic u-winds	UAG	17	m/sec
Ageostrophic v-winds	VAG	17	m/sec
Temperature	T	17	K
Bulk Richardson number	BRN	16	unitless
Pressure vertical velocity	W	12	Pa/sec
Relative humidity	RH	8	%

Equation (20), however, did not account for phenomena such as the shrinking area between latitude lines when moving toward the poles. This was compensated for by making the gradient and Coriolis parameter a function of latitude. The x and y components of the gradient, dx and dy, were made functions of latitude by transforming them into spherical coordinates (Holton, 1992:33):

$$dx = r_e \cos(\phi) d\lambda$$
$$dy = r_e d\phi \qquad\qquad (21)$$

where

ϕ = latitude (rad)

λ = longitude (rad)

r_e = radius of the earth (m).

The Coriolis parameter was also represented as (Holton, 1992:13,39):

$$f = 2\Omega \sin(\phi), \qquad\qquad (22)$$

where Ω is the angular frequency of the earth or 7.292 x 10^{-5} rad/sec.

Furthermore, the derivatives in the gradient were estimated using finite difference approximations or specifically, centered differences of order $(\Delta x)^2$ (Haltiner and Williams, 1980:109). The geostrophic wind components were then defined as:

$$V_{gx} = -\frac{1}{f}\frac{H(y+\Delta y) - H(y-\Delta y)}{2\Delta y}$$
$$V_{gy} = \frac{1}{f}\frac{H(x+\Delta x) - H(x-\Delta x)}{2\Delta x} \qquad (23)$$

where

V_{gx} = x component of the geostrophic wind

V_{gy} = y component of the geostrophic wind

Δy = meridional distance between grid points

Δx = zonal distance between grid points.

Finally, the difference in Equation (19) was computed and ageostrophic winds were obtained. Vectors of total wind, geostrophic wind and ageostrophic wind were also plotted in the Grad Analysis and Display System (GRADS) to ensure accuracy.

3.3.1.2 Bulk Richardson Number.

Theoretical work has shown that the Richardson number, a ratio between buoyancy and wind shear, can be used as an indicator of atmospheric turbulence (Stull, 1988:177). Since turbulent mixing is thought to cause fluctuations in the refractive index, the Richardson number may be an indicator of optical turbulence as well (Warnock and VanZandt, 1985:1).

If the Richardson number is less than about 0.25, then for the possibility for the onset of turbulence is high. This work was based only on local observations of the wind shear and temperature gradients. Local gradients, however, are seldom known, but estimates of the gradients can be made at discrete height intervals using finite differences. These estimates are included in a more realistic ratio called the bulk Richardson number.

The bulk Richardson number, BRN, is defined as (Stull, 1988, 177):

$$BRN = \frac{g \; \Delta \bar{\theta}_v \; \Delta z}{\bar{\theta}_v \left[\left(\Delta \bar{U} \right)^2 + \left(\Delta \bar{V} \right)^2 \right]}, \qquad (24)$$

31

where

g = acceleration due to gravity (m/sec^2)

$\overline{\theta}_v$ = mean virtual potential temperature (K)

Δz = height interval (m)

$\Delta \overline{U}$ = difference in mean zonal wind between two layers (m/sec)

$\Delta \overline{V}$ = difference in mean meridional wind between two layers (m/sec).

The differences in mean winds between two layers were estimated using U and V from the NCEP/NCAR database at two different pressure levels or:

$$\Delta \overline{U} \approx U(p_2) - U(p_1)$$
$$\Delta \overline{V} \approx V(p_2) - V(p_1)$$

where p_2 and p_1 are the pressures at the top and bottom layers, respectively. The other variables in (24) were derived from variables in Table 2 as shown below.

The height interval Δz was computed using the geopotential height H (List, 1951:218):

$$\Delta z = \frac{r_e H_2}{\left(\dfrac{g r_e}{9.8}\right) - H_2} - \frac{r_e H_1}{\left(\dfrac{g r_e}{9.8}\right) - H_1}, \qquad (25)$$

where H_2 is the geopotential height at the top layer and H_1 is the geopotential height at the bottom layer.

To calculate the mean virtual potential temperature $\overline{\theta}_v$ and the change in mean virtual potential temperature $\Delta \overline{\theta}_v$, an expression had to be found in terms of known variables.

First, the saturated vapor pressure was defined from the Goff-Gratch formula (Duffield and Nastrom, 1984:10):

$$e_s = 100(10^{(a-b-c+d-e)}) \, , \qquad (26)$$

where

e_s = saturated vapor pressure (Pa)

$a = 23.832241$

$b = 5.02808 \log T$

$c = 1.3816(10^{-7})(10^{11.334-0.0303998T})$

$d = 8.1328(10^{-3})(10^{3.49149-1302.8844/T})$

$e = 2949.076/T$

T = temperature (K).

Once the saturated vapor pressure e_s was calculated, it was substituted into the equation for saturated mixing ratio w_{sat}:

$$w_{sat} = \varepsilon \frac{e_s}{p - e_s} , \qquad (27)$$

where ε is equal to 0.622 and p is the pressure (Pa). Third, the mixing ratio w was found from (Duffield and Nastrom, 1984:12):

$$w = \frac{RH}{100} w_{sat} , \qquad (28)$$

where RH is the relative humidity in percent. Fourth, w and w_{sat} were put into the virtual potential temperature equation. In saturated or cloudy air, the virtual potential temperature θ_v was defined as:

33

$$\theta_v = \theta\left(1 + 0.61w_{sat} - w_L\right), \qquad (29)$$

where

$$\theta = T\left(\frac{P_o}{P}\right)^{0.286}$$

θ = potential temperature (K)

P_o = reference pressure (100,000 Pa)

w_L = liquid water mixing ratio.

In an unsaturated environment, θ_v was defined as (Stull, 1988:7):

$$\theta_v = \theta(1 + 0.61w). \qquad (30)$$

The virtual potential temperature calculated for each layer was used as an approximation for the mean virtual potential temperature since meteorological values were only available at discrete heights. Similarly, the difference in mean virtual potential temperature was estimated by the difference in virtual potential temperature between two different heights. Finally, the BRN in equation (24) was calculated.

Note that an expression for the liquid water mixing ratio in (29) was not defined. There was insufficient information to calculate the value and furthermore, the concept of the ABL is to fire upon missiles above clouds or above the region where saturated air is confined. Therefore, values for the BRN were flagged in regions of saturated air so they could be omitted in the final data set to be used in the regression analysis. In addition, BRN values were flagged in regions where the difference in mean wind was zero, which resulted in an infinite BRN value, so their values could also be deleted from the regression data set.

34

3.3.2 Optical Turbulence Data.

One of the factors needed to compare time series of data in regression analysis is that the independent and dependent variables be measured simultaneously. Since the C_n^2 and meteorological values were not measured simultaneously, a temporal adjustment was made to the C_n^2 data. In addition, spatial changes were made to the C_n^2 data as described below.

As shown in Table 1, a C_n^2 measurement is made every 3 minutes while the meteorological data was measured in 6-hour increments. Rather than trying to interpolate values for all the variables listed in Table 2, the C_n^2 values were averaged in 6-hour increments to coincide with the weather data. First, a quality control check was conducted on the measured C_n^2 values by the sponsor using a program developed by NCAR (Weber and Wuertz, Oct 91). Then, averages were calculated for 06Z, 12Z, 18Z and 00Z using data available three hours before and three hours after each time as summarized in Table 3. Since many of the C_n^2 measurements were missing or did not pass the quality control check, consideration was given to the number of observations available for each 6-hour time average. Therefore, averages were only calculated where a majority of the observations, at least 70%, was available.

Table 3. Time and hours used in to calculate optical turbulence averages.

TIME	HOURS USED IN AVERAGE
06Z	03Z-09Z
12Z	09Z-15Z
18Z	15Z-21Z
00Z	21Z-03Z

35

Spatial averages were also computed for the C_n^2 data, after the time averages were completed, for brevity in the data set. Samples of the data were vertically averaged at different increments and studied to determine an appropriate range. This range could smooth some small-scale features while still capturing large-scale features. An increment of 300 meters appeared to keep the most interesting features in the data. In addition, vertical averages were only computed between altitudes of about 10,000 to 15,000 meters. This range was chosen so the tropopause level would be included, and therefore, the jet stream would be included since it is most often confined to a region near the tropopause (Nastrom and Eaton, 1995:2137). The vertical levels used for optical turbulence data averages are shown in Table 4.

Table 4. Vertical levels used for optical turbulence data averages.

Level	Altitudes Averaged (m)
1	10,122-10,272
2	10,422-10,572
3	10,722-10,872
4	11,022-11,172
5	11,322-11,472
6	11,622-11,772
7	11,922-12,072
8	12,222-12,372
9	12,522-12,672
10	12,822-12,972
11	13,122-13,272
12	13,422-13,572
13	13,722-13,872
14	14,022-14,172
15	14,322-14,472
16	14,622-14,772
17	14,922-15,072

36

4. Data Description and Analysis

4.1 Data Description

The meteorological and optical turbulence data sets used in this study were taken from different archives. They are described below.

4.1.1 NCEP/NCAR Reanalysis Data Set.

The basic concept of the NCEP/NCAR reanalysis project used a fixed state-of-the-art analysis/forecast system and performed data assimilation using past data from 1957 to the present (reanalysis). This analysis/forecast system would then perform data assimilation into the future. This would enable climatologists to determine whether current climate irregularities are significant when compared to an extended reanalysis without changes in the data assimilation system (Kalnay and others, 1996:438). In addition, this 40-year reanalysis provides a quality data set appropriate for many studies such as this one.

The reanalysis archive was designed to be comprehensive, allowing research in budget studies, and easily accessible to users in need of extended periods of data. Since it was not possible to meet both design requirements in one archive, several archival formats are available (Kalnay and others, 1996:448). The meteorological data used in this research was taken from the main synoptic archive in a gridded binary format.

37

The main synoptic archive is the most comprehensive archive of the reanalysis. It includes analysis and first-guess fields at 00Z, 06Z, 12Z and 18Z on a 2.5° latitude and longitude grid (Kalnay and others, 1996:449). The reanalysis gridded fields are also categorized into classes, based on their influence by observations and models on the gridded variable. Variables extracted from the synoptic archive and their class are summarized in Table 5. An *A* denotes that the variable is strongly influenced by observations; therefore, it is the most dependable class. The letter *B* denotes that both models and observations have influence on the variable (Kalnay and others, 1996:448).

Table 5. Classification of synoptic archive variables used in this study.

VARIABLE	SYMBOL	CLASS
Surface pressure	PS	B
Temperature at tropopause	TT	A
Pressure at tropopause	PT	A
U-winds at tropopause	UT	A
V-winds at tropopause	VT	A
Wind shear at tropopause	SHT	A
Surface lifted index	LI	B
Best (4-layer index)	B	B
Temperature at max wind level	TM	A
Pressure at max wind level	PM	A
U-winds at max wind level	UM	A
V-winds at max wind level	VM	A
Pressure reduced to mean sea level	PR	A
Geopotential height	H	A
U-winds	U	A
V-winds	V	A
Temperature	T	A
Pressure vertical velocity	W	B
Relative humidity	RH	B

As mentioned in 3.3.1, the meteorological data provided by AFRL included latitudes between 10° and 65° N and the entire longitude grid. A smaller grid between 30°-35°N and 102°30'-110°W was extracted from this grid to coincide with the radar site. Data was provided in six hour increments beginning at 00Z for all months in 1991-1996 and for January-June 1997. There were no missing database values; however, values of the BRN calculated from the database were defined as missing for the reasons discussed in 3.3.1.2.

<u>4.1.2 Radar Data.</u>

The measurements made by the WSMR 50-MHz radar were obtained and evaluated through a quality control (QC) program conducted by the sponsor. The QC program was designed by NCAR (Weber and Wuertz, Oct 91). The logarithm of C_n^2 was provided for heights (above mean sea level) between 3,222 meters and 19,722 meters in 150 meter increments. The data was temporally and vertically averaged between about 10,000 and 15,000 meters and as described in 3.3.2.

The data was available for January-April 1993, July-September 1993 and January 1994. Within these dates, there were several missing data values or values that did not pass the QC check. Estimated dates for missing values or values that failed the QC check at various pressure levels are shown in Table 6.

Table 6. Estimated days where radar data was missing or failed QC check.

	Jan 93	Feb 93	Mar 93	Apr 93	Jul 93	Aug 93	Sep 93	Jan 94
Days	1-15	16-20 27-29	13-30	1-8 12-15 18-19 22-26	1-8 10-20	29-30	4-5	1-3 9-10

4.2 Data Analysis

Data analysis involved some autocorrelation of the reanalysis database and radar measured optical turbulence values. Autocorrelation was not as pertinent to the regression analysis as originally thought at the beginning of this study as explained below. Analysis also included checking that the variables were normally distributed and studying scatterplots of the optical turbulence data versus the reanalysis variables. The focus of the data analysis, however, was the multiple linear regression described in detail below.

4.2.1 Autocorrelation

Autocorrelation can be defined as the correlation of a variable with itself. In the case of temporal autocorrelation, correlations are run on the past and future values of a variable. These are also known as lagged correlations. They can be pictured by comparing two copies of a sequence of values with one of the sequences shifted by a unit of time. A lag-1 correlation, shifted one unit of time, is usually calculated to measure persistence; however, autocorrelations with lags greater than one can be useful also (Wilks, 1995:52). They can be used to help determine when a variable becomes independent or is no longer correlated with its past value. They can also be used to determine seasonality in a variable.

Autocorrelations are computed using the Pearson correlation equation. For a lag k, the autocorrelation coefficient r_k can be computed from (Wilks, 1995:53):

$$r_k = \frac{\sum\limits_{i=1}^{n-k}\left[\left(x_i - \bar{x}_-\right)\left(x_{i+k} - \bar{x}_+\right)\right]}{\left[\sum\limits_{i=1}^{n-k}\left(x_i - \bar{x}_-\right)^2 \sum\limits_{i=1}^{n-k}\left(x_i - \bar{x}_+\right)^2\right]^{1/2}}, \qquad (31)$$

40

where $\bar{x}_-$ and $\bar{x}_+$ denote the sample means from the first and last (n - k) data values, respectively. This equation is only valid for $0 \le k < n-1$.

The collection of autocorrelations for different lags is known as the autocorrelation function. This function is usually displayed graphically with the autocorrelation plotted as a function of lag k. Autocorrelations for the data sets were computed with the SAS statistics package. An example of the autocorrelation function is shown in Figure 3 for the meridional wind at the tropopause, VT, at 30° N 107°30'W using 1993 data. Each lag k is a 6 hour increment. It shows a gradual decay toward zero as the lag k increases which is expected for most meteorological variables. If the autocorrelation function did not decay toward zero after a short period, then accurate long term forecasts would be easy; long term forecasts would simply be a slight modification of the observation made several days prior (Wilks, 1995:54). Figure 3 also shows that the autocorrelation of VT is near zero or that VT is independent around lag 19, which is approximately 5 days.
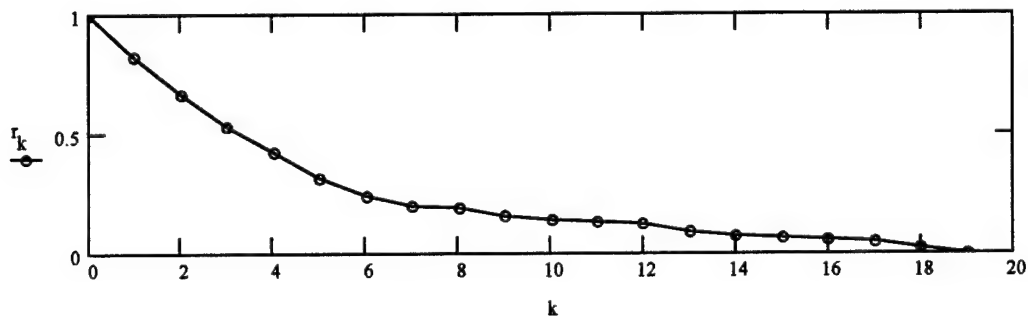
Figure 3. Autocorrelation function for VT at 30° N 107°30'W.

The autocorrelation function was used in this study because the original thought was that the variables used in the regression could not be serially correlated. However, this is

not the case. The variables can be strongly autocorrelated; however, the errors are assumed to be random and independent (refer to section 4.2.4.1). Therefore, the residuals, estimates of the error, cannot be highly autocorrelated (Wilks, 1995:174). In addition, there were several gaps and missing values in the final data sets used for the regression, so it did not make sense to perform autocorrelations on them. The final data sets were no longer a true time series of data due to missing months and days in the radar data and undefined bulk Richardson numbers. As a result, the autocorrelation functions produced were not pertinent to the multiple regression analysis and were not used further in this study.

4.2.2 Normality Check.

Since regression analysis usually assumes that its variables are normally distributed, this distribution was checked first. Note that this is not a requirement to complete a regression analysis. The Statistix and SAS computer packages used the Wilk-Shapiro measure to check for normality in both the optical turbulence and meteorological data. The Wilk-Shapiro value ranges from 0 to 1, with 1 representing a perfectly normal distribution. A graphical view of the Wilk-Shapiro measure will be a straight line for a value of Wilk-Shapiro value of 1. An example of the Wilk-Shapiro plot is shown in Figure 4 for the logarithm of C_n^2 representing the average around 10,500 meters. The Wilk-Shapiro value shown is 0.9204. In most cases, if the Wilk-Shapiro value is near 0.9, a normal distribution can be assumed.

Wilk-Shapiro values for the logarithm of the C_n^2 for heights between about 10,000 and 15,000 meters mostly fell near 0.9. All values were greater than 0.8, but some were closer

42

to 0.8 than to 0.9. For the purposes of this study, they were assumed to have a normal distribution.

A large sample of the meteorological variables was checked for normality at each grid point. The majority of the variables passed the normality check. There were a few variables which produced Wilk-Shapiro values near 0.8, such as relative humidity at different levels, but were still assumed to have a normal distribution.

Wilk-Shapiro / Rankit Plot of Log (C_n^2)
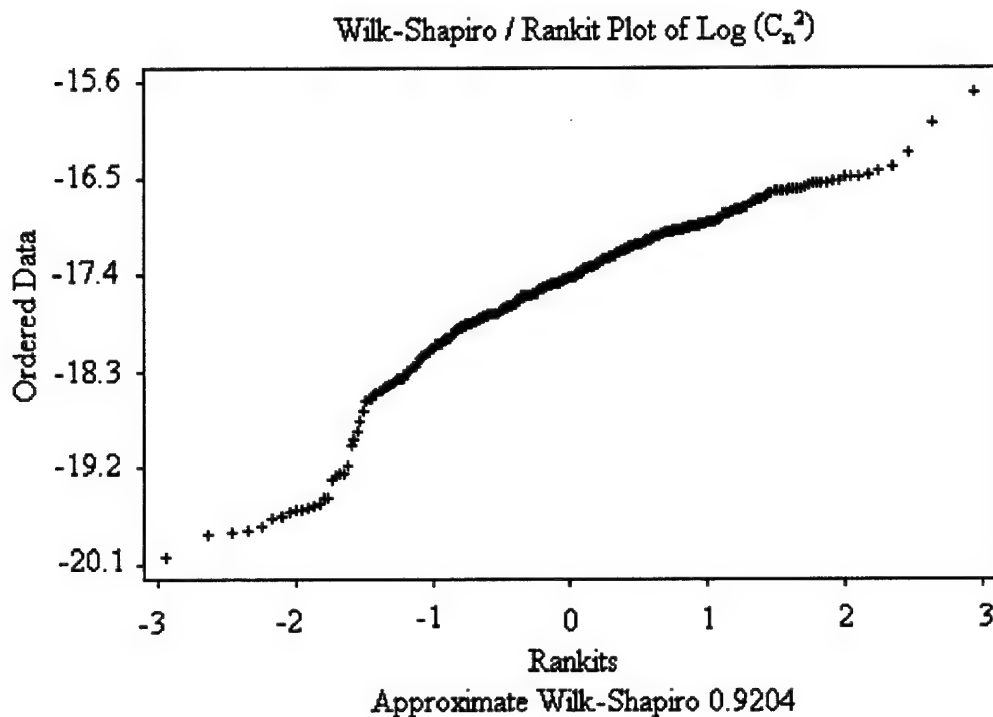
Figure 4. Wilk-Shapiro plot for log (C_n^2) around 10,500 m.

4.2.3 Graphical Analysis.

Scatter plots of the logarithm of C_n^2 versus the meteorological data were studied. This type of graphical analysis was used to gain initial insight into the linear relationship between the logarithm of C_n^2 and the reanalysis data.

43

Scatter plots for the logarithm of C_n^2 averaged around 10,500 meters versus various weather variables from January 15 to January 30 of 1993 are shown in Figure 5, Figure 6 and Figure 7. The approximated regression line is also displayed in the figures. A linear relationship is distinguishable in the scatter plot of the logarithm of C_n^2 versus zonal wind at the max-wind level (UM) depicted in Figure 6. A linear relationship is not as apparent, however, in Figure 5 and Figure 7. After studying several scatter plots for different grid points, it was determined that there was potential for a linear relationship between the synoptic scale weather variables and the logarithm of C_n^2.
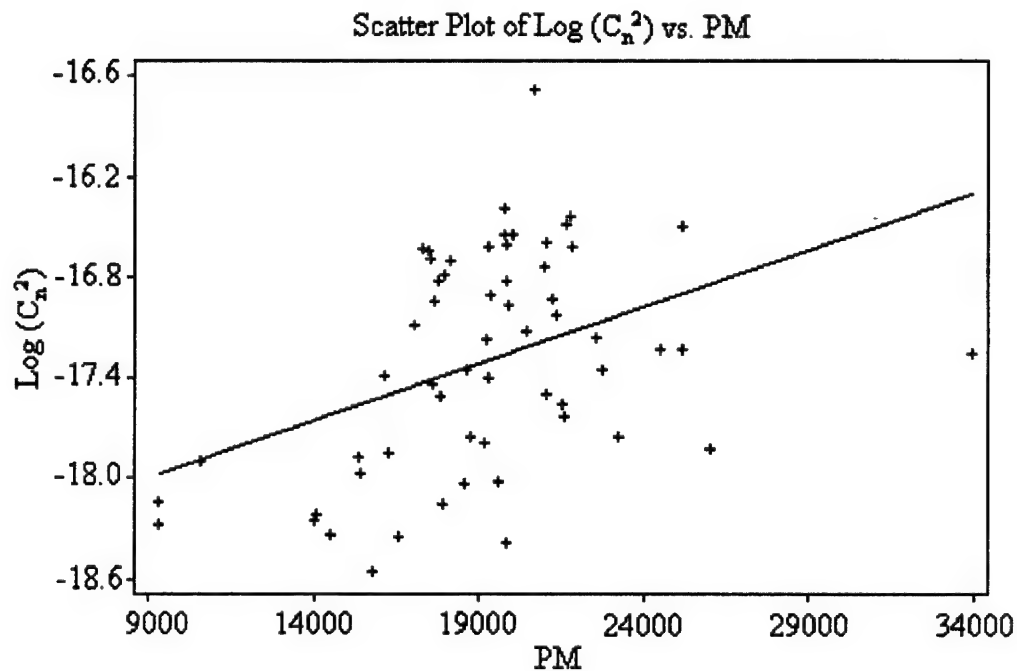
Figure 5. Scatter plot of log (C_n^2) vs. pressure at the max-wind level (PM).

44
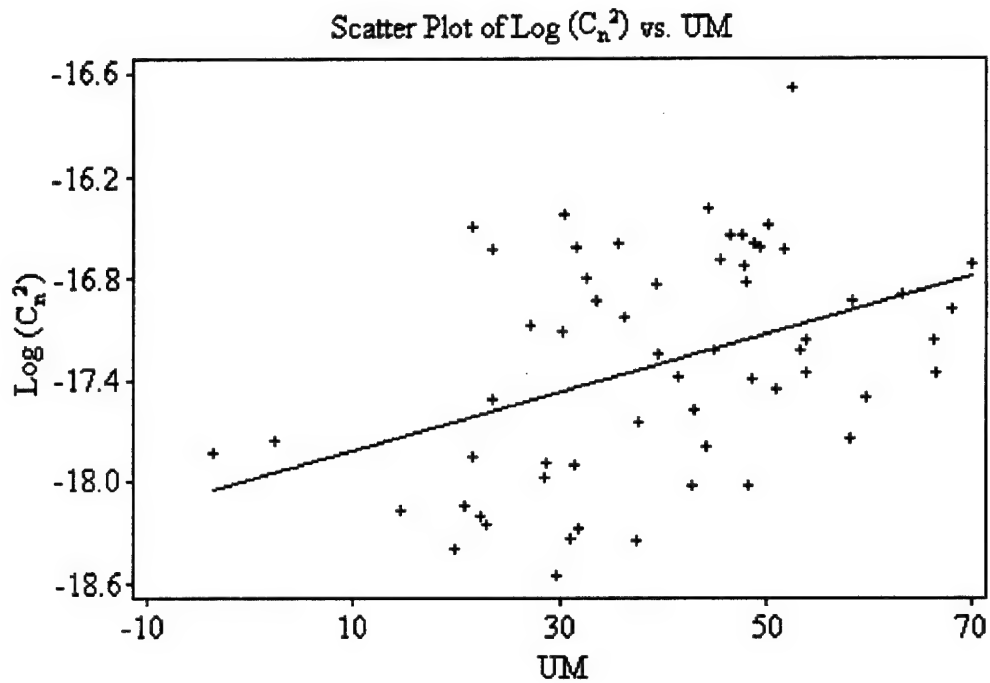
Figure 6. Scatter plot of log (C_n^2) vs. zonal wind at the max-wind level (UM).
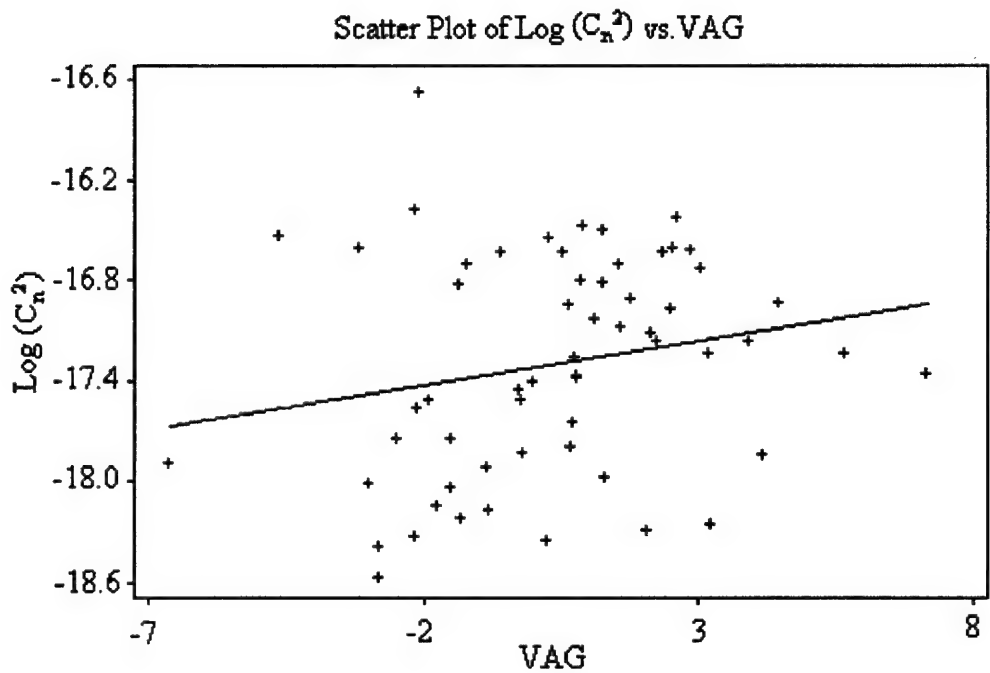
Figure 7. Scatter plot of log (C_n^2) vs. ageostrophic meridional wind at 925 mb (VAG).

45

4.2.4 Regression Analysis.

Regression analysis is a powerful statistical tool used to assess the relationship between one dependent variable and one or more independent variables. It is also useful because the independent variables can be somewhat correlated with one another (Tabachnick and Fidell, 1983:86).

Regression analysis is most easily explained by the case of simple linear regression, a special case of multiple linear regression (Wilks, 1995:160). This includes describing the analysis of variance, goodness-of-fit measures and the analysis of residuals. Regression analysis can then be easily expanded to the general case of multiple linear regression. If there are a large number of predictor variables, as in this study, then variable selection for the multiple linear regression can be automated using a stepwise technique.

4.2.4.1 Simple Linear Regression.

The concept of simple linear regression is to capture the relationship between two variables, given as x and y, in a single straight line. By convention, x is used for the independent or predictor variable and y is used for the dependent variable or predictand. The regression operation selects the line which produces the least error for predictions of y, given observations of x (Tabachnick and Fidell, 1983:87; Wilks, 1995:160; Devore, 1995:475). Least error usually means that the sum of squared errors is minimized.

Figure 8 depicts the situation. Given a data set of (x, y) pairs, the problem lies in determining the straight line which minimizes the vertical distance between the line and the data points. The equation for the line can be expressed as:

$$\hat{y} = a + bx, \qquad\qquad\qquad (32)$$

46

where $\hat{y}$ is the predicted value of y, a is the least-squares intercept and b is the slope of the line. The vertical distances between the data points and line, called residuals or estimates of the error, are defined as:

$$e_i = y_i - \hat{y}(x_i),\qquad\qquad\qquad (33)$$

where there is a different residual e_i for each data pair (x_i, y_i) (Wilks, 1995:160; Devore, 1995:485). It is assumed that the errors are independent, random variables with zero mean and constant variance. In addition, it is often assumed that the errors follow a normal distribution (Wilks, 1995:163).
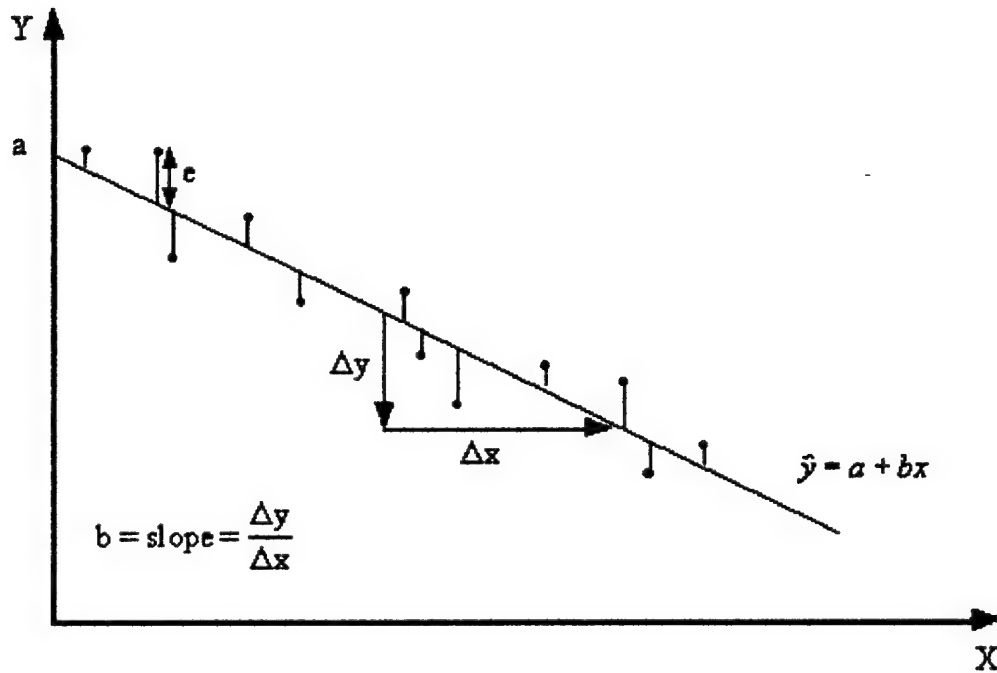
Figure 8. Schematic illustration of simple linear regression (Wilks, 1995:161).

Combining equations (32) and (33) gives the regression equation:

$$y_i = \hat{y}_i + e_i = a + bx + e_i,$$ (34)

which shows that the actual value of the predictand is the sum of the predicted value and residual (Tabachnick and Fidell, 1983:87; Wilks, 1995:161; Devore, 1995:477). In order to minimize the sum of squared errors, the least-squares intercept a and slope b in (34) must satisfy the following analytic expressions (Wilks, 1995:162):

$$b = \frac{n\sum_{i=1}^{n} x_i y_i - \sum_{i=1}^{n} x_i \sum_{i=1}^{n} y_i}{n\sum_{i=1}^{n}(x_i)^2 - \left(\sum_{i=1}^{n} x_i\right)^2}$$ (35)

$$a = \frac{1}{n}\left(\sum_{i=1}^{n} y_i - b\sum_{i=1}^{n} x_i\right)$$ (36)

where n is the number of data pairs.

4.2.4.2 Analysis of Variance.

In 4.2.4.1, the assumption of zero mean and constant variance in the errors was presented. This constant variance can be estimated using the residuals in:

$$s_e^2 = \frac{1}{n-2}\sum_{i=1}^{n} e_i^2,$$ (37)

where s_e^2 is the sum of squared residuals (Wilks, 1995:163).

Rather than calculating the sample variance from (37), it is more common to use a form based on the relationship:

$$SST = SSR + SSE,$$ (38)

48

where SST is the total sum of squares, SSR is the regression sum of squares and SSE is the sum of squared errors. SST can be defined as the sum of squared deviations of y around the mean of y or (Wilks, 1995:164):

$$SST = \sum_{i=1}^{n} (y_i - \bar{y})^2 , \tag{39}$$

where $\bar{y}$ is the mean of y. This is proportional to the estimated variance of y and, therefore, measures the overall variability of the predictand. The SSR term is the sum of squared differences between the regression predictions and the estimated mean of y or:

$$SSR = \sum_{i=1}^{n} [\hat{y}(x_i) - \bar{y}]^2 . \tag{40}$$

This can be related to the regression equation in (34) by:

$$SSR = b^2 \sum_{i=1}^{n} [x_i - \bar{x}]^2 , \tag{41}$$

where $\bar{x}$ denotes the mean of x. Finally, SSE is defined as the sum of squared differences between the residuals and their mean:

$$SSE = \sum_{i=1}^{n} e_i^2 . \tag{42}$$

The estimated error variance can now be shown as:

$$s_e^2 = \frac{1}{n-2}(SST - SSR) = \frac{1}{n-2} SSE \tag{43}$$

The output from many statistical computer packages includes the analysis of variance (ANOVA) parameters just described, in an ANOVA table. A generic form of the

49

ANOVA table is shown in Table 7. It includes the source of the variance in column 1, the degrees of freedom (DF) in column 2, the sum of squared (SS) values in column 3 and the mean squared (MS) values in column 4. The three rows comprise the error, regression and total values for each column. Note that error and regression values in the DF and SS columns will sum to the corresponding value in the total row (Wilks, 1995:165). The MS values are given by the corresponding values of SS/DF. For simple linear regression, there is one regression degree of freedom, so *SSR* is equal to the mean square of regression, MSR. Also, it was just shown that $s_e^2 = SSE/DF$, so s_e^2 is also equal to the mean squared error, MSE. The other value in the MS column, the F ratio, is a measure of the fit of a regression. This will be discussed further in 4.2.4.3.

Table 7. ANOVA Table for Simple Linear Regression (Wilks, 1995:166).

SOURCE	DF	SS	MS
Total	n - 1	SST	
Regression	1	SSR	MSR = SSR / 1 (F = MSR / MSE)
Error	n - 2	SSE	$MSE = s_e^2$

4.2.4.3 Goodness-of-Fit Measures.

Several measures can be used to determine the fit of a regression, or how well the regression line portrays the scatter plot of the data. Three commonly used measures of regression fit are the mean squared error, MSE, the coefficient of determination or R^2, and the F ratio.

The MSE is probably the most basic of the three measures since it shows the variability

of the observed y values around the regression line. Since MSE = s_e^2, this shows how the

residuals will fall around the regression line. If MSE is small, the residuals will be in close

proximity to the regression line and will most likely provide a good fit as shown in Figure

9 (Wilks, 1995:166). If MSE is large, they will be spread further from the regression line

and will be more likely to provide a unsatisfactory regression as illustrated in Figure 10.
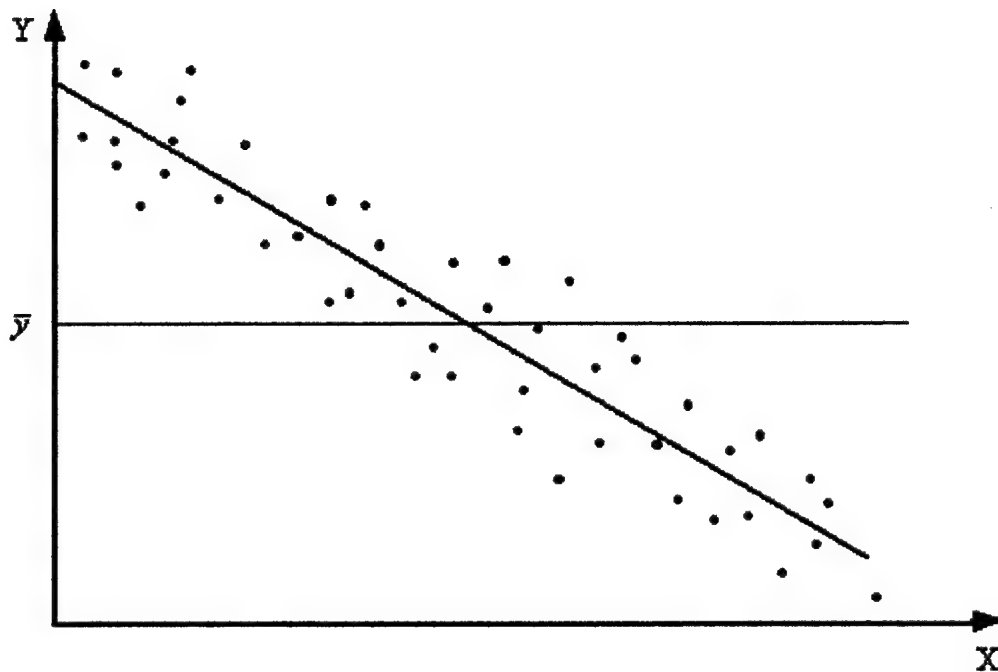
Figure 9. Small MSE indicating a fairly good regression relationship (Wilks, 1995:167).
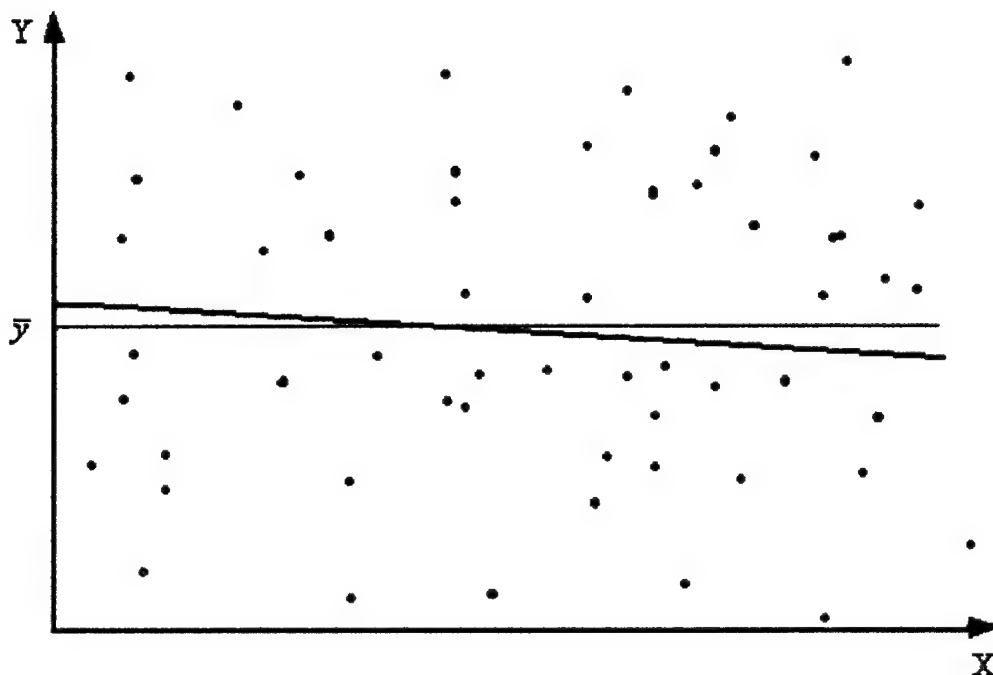
Figure 10. Large MSE showing a poor regression relationship (Wilks, 1995:167).

The second measure of the strength of a regression is the coefficient of determination or R^2. This can be calculated from:

$$R^2 = \frac{SSR}{SST} = 1 - \frac{SSE}{SST} \tag{44}$$

R^2 is understood to be the proportion of the variability of the predictand that is accounted for or explained by the regression (Devore, 1995:489). For a perfect regression, $SSR = SST$, $SSE = 0$, therefore $R^2 = 1$. For a worthless regression, $SSR = 0$, $SSE = SST$, therefore $R^2 = 0$. Figure 10 can also exemplify this poor case of regression as a R^2 value close to zero (Wilks, 1995:167).

The third measure of fit of a regression is the F ratio. As shown in Table 7, F is equal to the ratio of MSR to MSE; therefore, F increases with the strength of the regression, since a strong relationship between x and y generates a large MSR and small MSE (Wilks,

52

1995:168). It is based upon the F distribution which has two parameters. The first

parameter is the number of numerator degrees of freedom and the second is the number of

denominator degrees of freedom. A typical F density curve is shown in Figure 11 with a

corresponding upper tail critical value, F_c. The area to the right of the critical value under

the curve represents the significance level, α, of the test usually assumed to be 5% or 0.05.

In the SAS statistics package, the F ratio is for testing under the null hypothesis that all

parameters other than the intercept is zero. The alternate hypothesis is that at least one of

the parameters is not zero. If the F ratio is less than F_c or if the probability value (p-value)

of F is greater than α, then there is not enough evidence to reject the null hypothesis.

Therefore, the predictors do not contribute to the regression.
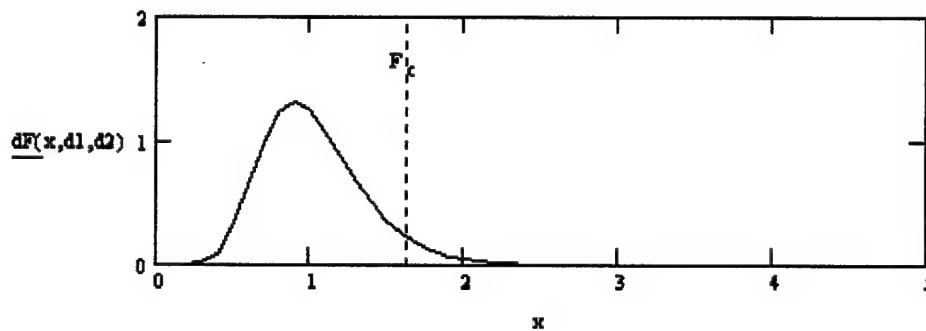
Figure 11. An example of the F distribution curve (Devore, 1995:397).

4.2.4.4 Analysis of Residuals.

Some of the results of statistics software packages can be misleading if the underlying

assumptions related to errors are not satisfied. As stated in 4.2.4.1, errors were assumed

to be independent, random variables with zero mean and constant variance, also called

homoscedasticity. In addition, the errors were assumed to have a normal distribution. These assumptions can be checked using estimators of error or residuals.

An easy and basic check on residuals can be made by examining a scatter plot of the residuals, e, against the predicted values, $\hat{y}$ (Tabachnick and Fidell, 1983:93; Wilks, 1995:171). If the residuals give the appearance of a horizontal band around their zero mean as illustrated in Figure 12, then the assumption of homoscedasticity is supported (Wilks, 1995:172).

The Wilk-Shapiro measure may be used to determine whether the residuals follow a normal distribution. If the Wilk-Shapiro value is near 0.9 with a near linear plot, a normal distribution of the residuals can be assumed.

Finally, the independence of residuals can be checked if the original data was temporally correlated. A plot of the residuals as a function of time can be examined. If groups of positive and negative residuals tend to bunch together, rather than occurring more randomly, then serial correlation can be suspected. The Durbin-Watson test statistic may also be used. This test examines the null hypothesis that the residuals are serially correlated against the alternate hypothesis that they are consistent with a first-order autoregressive process. The Durbin-Watson test statistic, d, can be expressed as:

$$d = \frac{\sum_{i=2}^{n}(e_i - e_{i-1})^2}{\sum_{i=1}^{n}e_i^2} \qquad (45)$$

This statistic basically calculates the squared differences between pairs of successive residuals and divides them by a scaling factor. If the residuals are positively correlated, d

will be relatively small (Wilks, 1995:173). If the residuals are randomly distributed in time, then d will be relatively large. As mentioned in 4.2.1, even though a regression uses strongly autocorrelated variables for both predictand and predictors, the residuals will not necessarily be strongly autocorrelated themselves (Wilks, 1995:174).
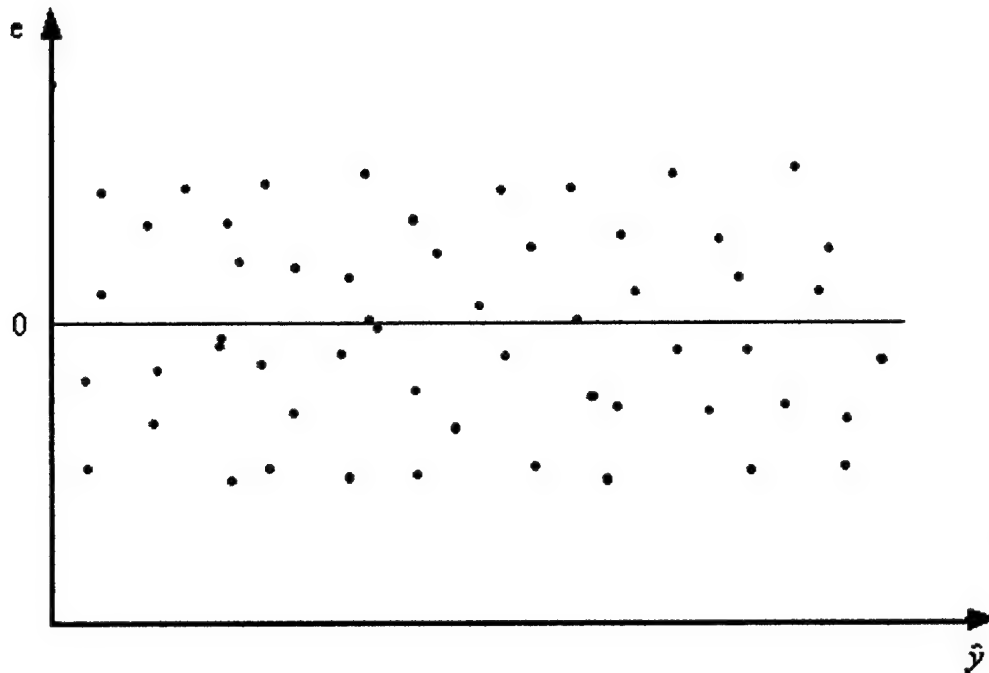
Figure 12. Scatter plot of residuals vs. predicted values (Wilks, 1995:172).

4.2.4.5 Multiple Linear Regression.

Multiple linear regression is the more general case of linear regression. It is similar to simple linear regression where there is a predictand, y, but there is more than one predictor variable, x. The previous discussion of simple linear regression will generalize to the situation of multiple linear regression.

Let K be the number of predictor variables. Simple linear regression was just the special case where $K = 1$. The prediction equation for multiple linear regression can then be given as:

$$\hat{y} = b_o + b_1 x_1 + b_2 x_2 + \ldots + b_K x_K, \qquad (46)$$

where b_o is the intercept, b_K is the coefficient, comparable to the slope, for each predictor variable x_K (Wilks, 1995:176; Devore, 1995:550).

Equation (33) for the residuals still applies; however, the fact that the predicted value $\hat{y}$ is a function of a vector of predictors, x_K, must be taken into account. If there are two predictor variables, $K = 2$, then the residual can still be pictured as a vertical distance from the regression surface, rather than just a line. For more than two predictors, the geometric situation is similar, but difficult to picture.

The $(K + 1)$ parameters are found similarly to simple linear regression by minimizing the sum of squared errors. This is done most easily by solving simultaneous equations using matrix algebra or by using statistical software packages. The results can also be summarized in an ANOVA table for multiple regression as shown in Table 8. Notice that the calculations are analogous to those in simple linear regression with the only difference being the degrees of freedom.

Table 8. ANOVA Table for Multiple Linear Regression (Wilks, 1995:177).

SOURCE	DF	SS	MS
Total	n - 1	SST	
Regression	K	SSR	MSR = SSR / K (F = MSR / MSE)
Error	n - K - 1	SSE	MSE = SSE / (n - K - 1) = s_e^2

<u>4.2.4.6 Stepwise Regression.</u>

Multiple regression analysis seems to enable an endless number of potential predictor variables. An initial list can be multiplied significantly by using mathematical transformations such as the square of predictors or products of predictors, called interaction terms (Wilks, 1995:177; Devore, 1995:553). In this study, there are 151 potential predictors (shown in Table 2) with approximately 2.85×10^{45} (2^{151}) combinations of models. With such a large number of predictors, explicit examination of all possible subsets is impossible, especially within the three months this study was conducted. There are however, alternative methods that can be used to identify good regression models (Devore, 1995:571). The method chosen for this study was stepwise regression.

Stepwise regression uses a combination of a forward selection and backward elimination method. The procedure starts by adding predictor variables to the model one by one. After each addition, the statistics package examines those variables previously entered to determine if they are still statistically significant to the model. If they are no longer significant, they are eliminated from the model (Devore, 1995:576). In the SAS statistics package, predictor variables are examined for addition or deletion based on an F statistic at the 0.15 significance level.

Stepwise regression was chosen for many reasons. First, parsimony where less is more in terms of predictors, was a major goal for each model (Cody and Smith, 1991:220). Stepwise regression would ensure that each variable provided a significant contribution to the model rather than just trying to obtain the largest coefficient of determination with insignificant predictors. Since the coefficient of determination increases with the number

57

of predictor variables, this would most likely produce an overfit model (Devore, 1995:572). Stepwise regression would also ensure that insignificant predictors were omitted, unlike either the forward selection or backward elimination procedure. Second, with the number of potential predictors, computing processing time would not be a problem. A procedure to find the largest coefficient of determination was available; however, it finds R^2 values for all possible combinations of the model. As mentioned previously, this was not an option due to the large number of potential predictors. Finally, there is a smaller chance of multicollinearity, or high correlation between predictors which can give misleading results when using stepwise regression.

5. Findings and Conclusions

5.1 Results

Results of the stepwise regression procedure for latitudes and longitudes between 30-35°N, 102°30'-110°W indicate a weak linear relationship between the logarithm of C_n^2 at various altitudes with different synoptic scale meteorological variables. This was confirmed by first validating results through analysis of residuals and then by examining the R^2 values, the MSE terms and the F ratios.

Analysis of residuals was conducted by first examining scatter plots of residuals versus predicted values, to ensure the assumption of homoscedasticity in the errors was met. Analysis of residuals then included testing the assumption of normality using the Wilk-Shapiro normality test. The assumptions of homoscedasticity and normality in the errors appeared to be supported. The Durbin-Watson test for serial correlation of the data was not conducted because the data used in the regression analysis was not a true time series. Since testing variables for independence with several gaps in the data did not make sense, it was assumed that the errors were independent and random.

The R^2 values for all the regression models are summarized in Table 9. They are arranged in latitude and longitude coordinates versus averaged vertical level given in Table 4. All R^2 values are statistically significant at the 0.05 significance level. The values range from 0.130 (35°N, 102°30'W, level 16) to 0.682 (32°30'N, 107°30'W, level 9), which is relatively distant from the R^2 value of 1 indicating a perfect regression; however, the majority of the values are near 0.5 indicating a weak relationship. Further examination

59

of Table 9 shows that the highest values, where the strongest linear relationship can be assumed, fall between levels 7 through 12 or altitudes of about 12,000 to 13,500 meters. The three highest R^2 values are located between levels 9 and 11 (altitudes of approximately 12,600 to 13,200 meters) at 32°30'N, 107°30'W, which is the grid point located closest to the radar site at 32°24'N, 106°21'W. Lowest values, indicating the weakest relationships, are between levels 16 and 17 or altitudes of about 14,600 to 15,000 meters, respectively.

Table 9. R^2 values for latitude/longitude coordinates vs. averaged vertical level.

(°N) (°W)	30 102.5	32.5 102.5	35 102.5	30 105	32.5 105	35 105	30 107.5	32.5 107.5	35 107.5	30 110	32.5 110	35 110
LEVEL												
1	.487	.492	.503	.586	.524	.541	.594	.596	.451	.608	.567	.503
2	.522	.554	.557	.556	.602	.526	.536	.609	.583	.481	.617	.539
3	.494	.527	.511	.524	.489	.540	.535	.534	.539	.529	.542	.559
4	.493	.524	.506	.481	.597	.466	.509	.520	.522	.556	.566	.484
5	.562	.480	.477	.578	.581	.434	.610	.564	.532	.577	.606	.557
6	.408	.504	.374	.587	.562	.430	.591	.584	.502	.508	.609	.596
7	.427	.542	.429	.432	.619	.522	.589	.606	.526	.520	.30	.565
8	.499	.581	.528	.565	.671	.493	.623	.551	.565	.508	.583	.542
9	.477	.451	.577	.578	.596	.548	.632	.682	.623	.637	.580	.594
10	.457	.465	.505	.514	.613	.559	.580	.677	.584	.612	.574	.550
11	.450	.432	.415	.435	.571	.506	.602	.668	.623	.615	.635	.609
12	.404	.413	.444	.505	.605	.463	.578	.555	.514	.552	.527	.608
13	.497	.266	.394	.436	.450	.454	.535	.525	.238	.500	.477	.306
14	.346	.196	.209	.442	.489	.334	.548	.517	.436	.419	.476	.394
15	.324	.286	.292	.333	.441	.249	.394	.526	.306	.507	.468	.413
16	.361	.201	.130	.396	.353	.219	.367	.376	.313	.250	.257	.351
17	.319	.198	.305	.364	.277	.269	.306	.351	.238	.315	.346	.357

The MSE values shown in Table 10 range from 0.104 (30°N, 105°W, level 17) to 0.324 (30°N, 102°30'W, level 7). The MSE terms appear to be relatively small; however, it is difficult to visualize the MSE using the distance from the residuals to the regression

surface with so many predictors, so the F ratio was used to test for the linear relationship that may exist between $\log (C_n^2)$ and the weather variables.

Table 10. MSE values for latitude/longitude coordinates vs. averaged vertical level.

(°N) (°W)	30 102.5	32.5 102.5	35 102.5	30 105	32.5 105	35 105	30 107.5	32.5 107.5	35 107.5	30 110	32.5 110	35 110
LEVEL												
1	.265	.263	.260	.224	.250	.244	.230	.223	.269	.225	.242	.262
2	.255	.243	.255	.244	.219	.256	.253	.224	.221	.282	.222	.262
3	.259	.253	.271	.241	.269	.247	.257	.251	.242	.252	.252	.246
4	.244	.246	.258	.256	.210	.271	.258	.238	.239	.235	.235	.262
5	.203	.247	.246	.206	.197	.258	.196	.209	.203	.202	.200	.213
6	.291	.256	.320	.216	.234	.274	.226	.226	.238	.256	.215	.218
7	.324	.262	.317	.314	.226	.262	.247	.223	.254	.273	.218	.240
8	.275	.236	.255	.229	.196	.264	.216	.238	.240	.260	.229	.259
9	.243	.256	.206	.193	.195	.213	.179	.160	.183	.178	.204	.200
10	.223	.221	.201	.194	.172	.177	.178	.139	.174	.160	.176	.189
11	.235	.244	.251	.230	.201	.209	.184	.151	.169	.177	.168	.184
12	.231	.222	.215	.192	.169	.197	.175	.191	.183	.176	.187	.170
13	.202	.263	.229	.212	.209	.204	.187	.195	.280	.191	.195	.262
14	.240	.283	.286	.209	.203	.250	.185	.199	.219	.221	.206	.233
15	.218	.236	.229	.191	.191	.215	.212	.188	.204	.173	.188	.204
16	.135	.162	.186	.139	.128	.159	.142	.143	.136	.155	.154	.137
17	.117	.134	.112	.104	.123	.114	.120	.113	.137	.114	.109	.118

The F test shown below was conducted on the regression model with the largest R^2 value of 0.682. This model was for the grid point at 32°30'N, 107°30'W at an altitude of about 12,600 meters. The ANOVA table for this regression model, which includes the F statistic and its corresponding probability value (p-value), is given in Table 11.

Table 11. ANOVA table for 32°30'N, 107°30'W, 12,600 m.

SOURCE	DF	SS	MS
Total	263	115.541	
Regression	34	78.803	2.318 (F = 14.45, p-value = 0)
Error	229	36.738	0.160

61

The assumptions of homoscedasticity and normality in the errors were checked first to ensure that the results from the SAS statistics package were valid for this grid point. The scatter plot of residuals versus predicted values of log (C_n^2), plotted using SAS, is shown in Figure 13. There appears to be an equal amount of variance above and below zero or the expected value of the error. The general shape of a horizontal band around the zero line can be seen; therefore, the assumption of homoscedasticity is supported. The Wilk-Shapiro plot of the residuals is shown in Figure 14. The plot shows a strong linear fit with a Wilk-Shapiro value of 0.9970; therefore, the assumption of normality is strongly supported. The model results from the SAS package were then deemed valid and the F test was conducted.

```
        ---+---------+---------+---------+---------+---------+---------+---
RESIDUAL |                                                               |
R     1 +                    o             ooo                           +
e       |              o           o oo oo  o  o ooo    o o oo            |
s       |               o     o o oo  oooooooooooooooooooo      o     o o |
i     0 +                    o    oooooo oooooooooooooooooooooooooooo     +
d       |       oo   oo           oo   oo oooo ooooooooo  oooooooooooooo o|
u       |     oo o ooo oo                o ooo    ooo  o    o oo  o      o |
a    -1 +              o                                                  +
l       |                       o                                        |
        |                                                                |
     -2 +                                                                +
        ---+---------+---------+---------+---------+---------+---------+--- .
           -19.5     -19.0     -18.5     -18.0     -17.5     -17.0     -16.5
                    Predicted Value of LCN          PRED
```
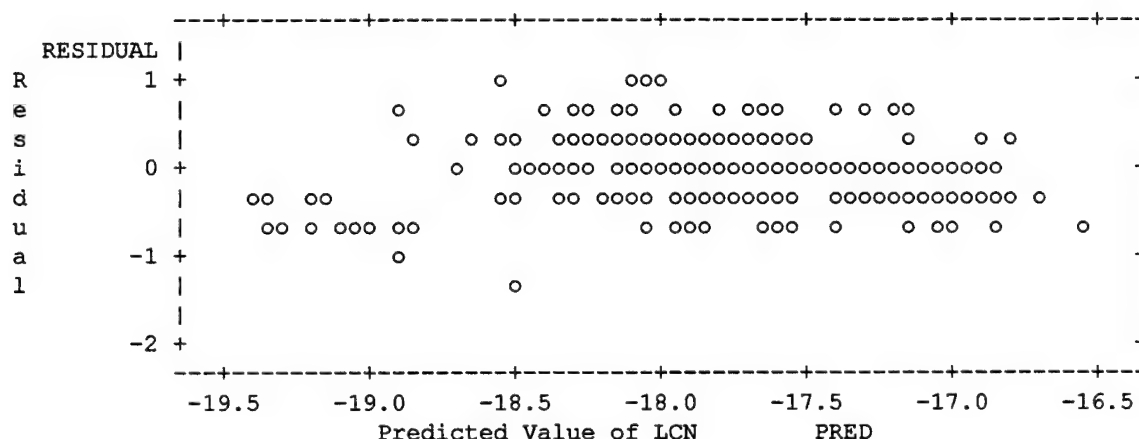
Figure 13. Scatter plot of residuals vs. predicted values (32°30'N, 107°30'W, 12,600 m) .

The null hypothesis for this F test is that all parameters except for the intercept are zero. The alternate hypothesis is that at least one parameter is not zero. The situation is illustrated in Figure 15. First, an F distribution curve was plotted using the regression

degrees of freedom, 34, as d1 and the error degrees of freedom, 229, as d2. Assuming a significance level α of 0.05, a critical value of F, denoted F_c, was also computed. Since $F = 14.45$ is larger than $F_c = 1.481$ or the corresponding p-value = 0 is less than $\alpha = 0.05$, the null was rejected. Therefore, the independent variables contribute to the regression or to predicting values of log (C_n^2).
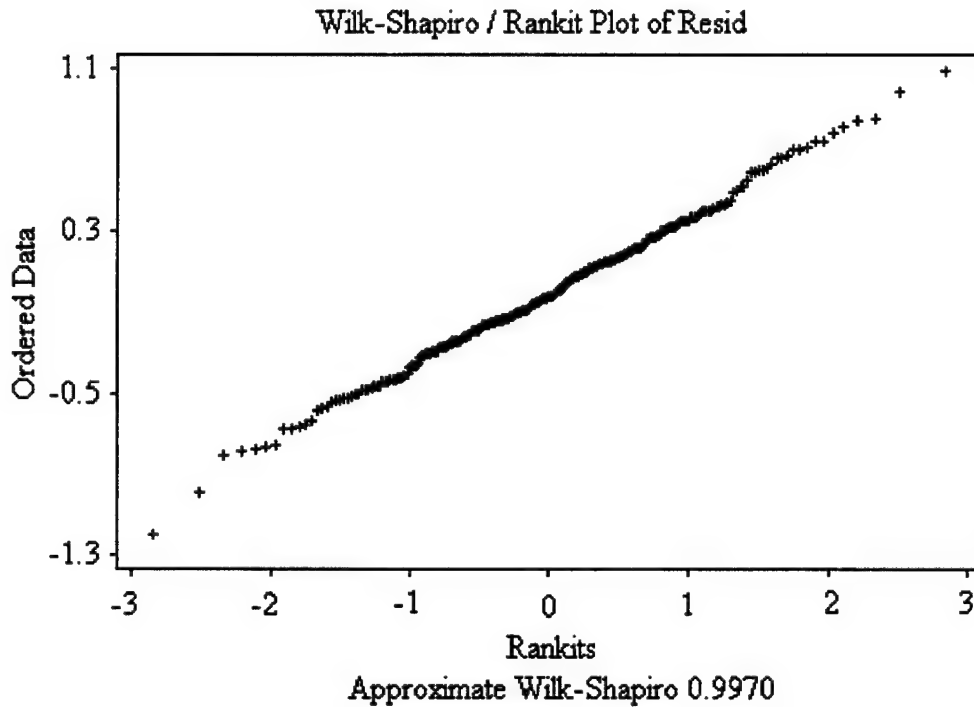
Figure 14. Wilk-Shapiro plot of residuals (32°30'N, 107°30'W, 12,600 m).

F ratios and their corresponding p-values for all regression models are summarized in Table 12. Shorthand notation was used for p-values less than zero with E representing the power of 10 (for example, $3E-16 = 3 \times 10^{-16}$). All F ratios are all statistically significant assuming a 0.05 significance level. In other words, the meteorological variables contribute to the regression or to predicting values of log (C_n^2) for all models.
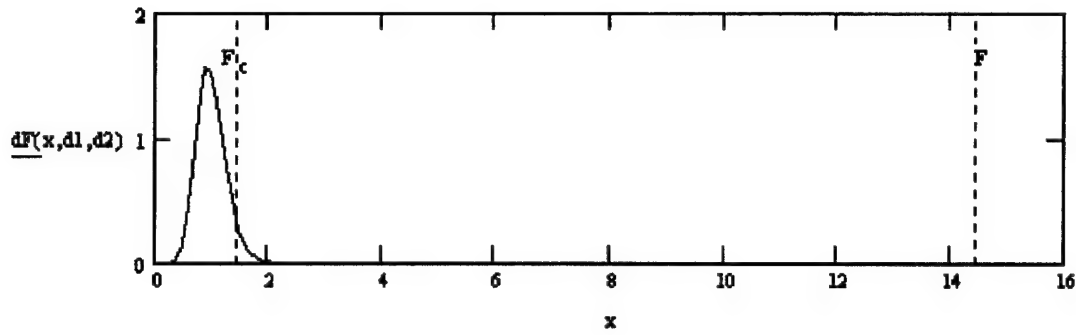
Figure 15. F distribution curve for 32°30'N, 107°30'W, 12,600 m.

The number of predictors in each model, summarized in Table 13, varied from 7 up to 42 variables. Most models with a large number of predictors showed a relatively high R^2 value while models with a small number of predictors showed a low R^2 value. The number of predictors was the lowest at levels 16 and 17. There was no apparent trend between the number of predictors and mean squared error.

A plot of predictor variables versus their frequency of occurrence in all regression models is shown in Figure 16. The last nine predictors have frequencies much greater than the first 13 variables because they are available at several different pressure levels. The predominant variables were temperature, mid and upper level wind and ageostrophic wind components and the bulk Richardson number. A list of the top 10 predictors in descending order of frequency is given in Table 14. The total wind, ageostrophic wind and bulk Richardson number were expected to be predictors of C_n^2 as stated in 2.3. The temperature was not expected to be a predictor based on the literature; however, based on theory, it is logical that temperature would be a included as a predictor of C_n^2 because the refractive index depends on temperature for electromagnetic waves. The refractive index is also a function of humidity, but near the stratosphere, the humidity can be considered

64

negligible. The wind components at the tropopause did not contribute to most models as predicted. This is probably due to the fact that the wind at the tropopause is highly correlated with mid and upper level winds.

Table 12. F and p-values for latitude/longitude coordinates vs. averaged vertical level.

(°N) (°W)	30 102.5	32.5 102.5	35 102.5	30 105	32.5 105	35 105	30 107.5	32.5 107.5	35 107.5	30 110	32.5 110	35 110
LEV												
1	13.45	13.19	17.9	12.49	18.11	14.38	13.81	14.82	17.94	12.07	15.98	13.10
	0	0	0	0	0	0	0	0	0	0	0	0
2	10.93	11.40	11.61	12.10	13.76	12.76	14.59	13.90	10.80	13.57	14.47	13.03
	0	0	0	0	0	0	0	0	0	0	0	0
3	12.17	11.59	10.26	11.78	16.76	12.51	12.92	14.23	11.71	14.94	13.04	11.18
	0	0	0	0	0	0	0	0	0	0	0	0
4	18.04	11.23	9.41	16.58	13.06	11.14	14.18	15.18	12.56	12.88	13.42	11.08
	0	0	0	0	0	0	0	0	0	0	0	0
5	13.00	10.68	12.94	10.64	13.60	10.53	12.55	13.53	12.33	13.58	11.94	11.15
	0	0	0	0	0	0	0	0	0	0	0	0
6	10.22	7.54	11.26	10.54	11.16	11.16	11.82	12.70	12.54	13.30	14.42	12.14
	0	0	0	0	0	0	0	0	0	0	0	0
7	8.57	9.83	8.09	10.51	10.32	11.46	10.71	14.85	12.35	9.90	13.09	14.82
	0	0	0	0	0	0	0	0	0	0	0	0
8	10.62	11.97	10.07	12.33	12.63	13.84	11.93	15.96	12.34	14.35	13.47	14.04
	0	0	0	0	0	0	0	0	0	0	0	0
9	8.85	10.09	10.09	11.06	14.28	12.41	13.53	14.45	12.97	11.98	12.98	14.69
	0	0	0	0	0	0	0	0	0	0	0	0
10	8.22	9.44	7.20	10.62	10.66	10.02	12.37	14.65	11.91	12.71	12.88	15.42
	0	0	0	0	0	0	0	0	0	0	0	0
11	10.45	9.73	8.71	9.50	11.79	10.91	15.08	14.74	12.16	11.04	14.24	13.32
	0	0	0	0	0	0	0	0	0	0	0	0
12	7.93	9.73	11.25	8.58	10.81	10.41	11.84	11.42	10.50	11.21	11.00	11.47
	0	0	0	0	0	0	0	0	0	0	0	0
13	6.84	8.88	6.36	8.76	8.73	7.97	9.87	9.73	11.27	8.69	10.88	13.31
	0	2E-13	9E-16	0	0	0	0	0	2E-12	0	0	7E-16
14	6.68	5.82	6.74	7.58	7.78	6.00	11.02	9.98	7.91	9.26	8.78	10.05
	1E-14	2E-8	3E-9	0	0	3E-13	0	0	0	0	0	0
15	6.01	5.71	6.19	5.72	8.12	5.32	8.76	9.03	8.49	8.32	8.43	8.07
	2E-12	7E-11	2E-11	6E-12	0	3E-9	0	0	3E-13	0	0	1E-15
16	6.69	5.29	5.77	7.29	6.80	5.38	6.89	7.13	5.64	6.08	7.03	8.72
	1E-15	2E-8	3E-6	0	2E-15	5E-9	3E-16	4E-16	6E-12	6E-11	1E-11	3E-15
17	8.63	8.79	7.74	6.45	9.01	8.32	5.95	7.24	9.14	8.01	8.23	8.12
	3E-16	1E-10	2E-14	2E-15	1E-14	2E-13	6E-13	2E-15	5E-12	1E-15	1E-16	3E-16

Table 13. Number of predictor variables in each regression model.

(°N) (°W)	30 102.5	32.5 102.5	35 102.5	30 105	32.5 105	35 105	30 107.5	32.5 107.5	35 107.5	30 110	32.5 110	35 110
LEVEL												
1	24	25	19	36	20	27	35	31	15	42	27	24
2	32	35	34	32	35	28	26	34	38	23	35	27
3	26	31	32	29	19	30	29	25	30	25	29	33
4	17	30	32	17	34	24	23	21	25	30	29	24
5	28	25	20	35	29	21	35	26	25	29	35	29
6	19	36	15	35	31	19	33	29	21	22	29	30
7	23	31	24	19	39	25	34	26	22	29	33	21
8	24	29	27	26	39	18	34	19	25	19	26	20
9	26	21	32	30	26	24	31	34	30	36	26	23
10	25	23	33	24	35	30	27	32	27	30	25	18
11	20	20	20	20	28	23	25	31	31	35	29	26
12	22	19	18	29	35	21	29	26	24	28	25	30
13	35	11	25	22	24	26	29	27	7	29	21	8
14	20	11	10	25	30	21	27	25	23	20	25	15
15	19	17	16	20	23	15	18	27	12	29	24	19
16	22	13	7	23	21	14	22	21	20	15	13	15
17	15	8	15	23	12	12	20	19	9	16	17	17

5.2 Conclusions

This study has shown that a linear relationship exists between the NCEP/NCAR

reanalysis database variables and the averaged logarithm of C_n^2 values measured at WSMR

for a discontinuous period between January 1993 to January 1994. The strongest

relationships found were located closest to the radar site, which was somewhat intuitive.

The most significant predictors in this study were temperature, total and ageostrophic

wind components and the bulk Richardson number. This study also showed that although

a linear relationship exists, this relationship is a weak one with several complicated

regression models.

Based on the results, it was concluded that the exact relationship between optical turbulence and synoptic scale variables could not be defined at this time; further research was needed. Suggestions that may strengthen this relationship is provided next.
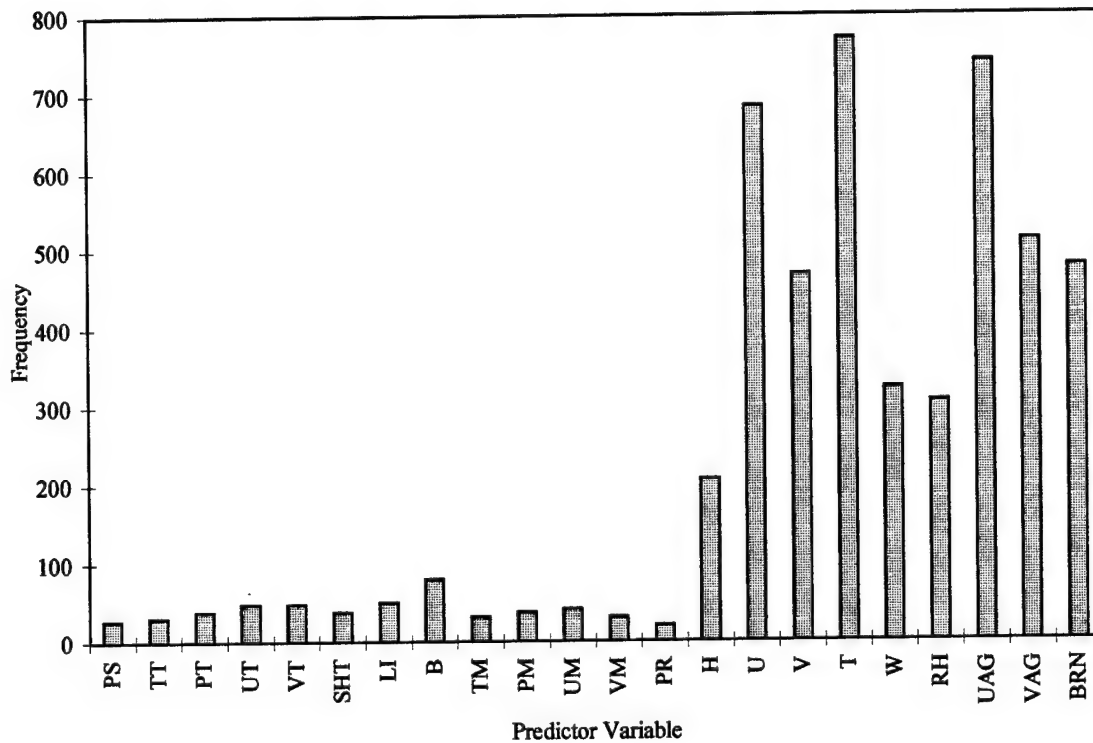

Figure 16. Predictor variable vs. frequency of occurrence in all regression models.

Table 14. Top 10 predominant predictor variables in descending order of frequency.

VARIABLE	SYMBOL
Temperature	T
Ageostrophic u-winds	UAG
U-winds	U
Ageostrophic v-winds	VAG
Bulk Richardson number	BRN
V-winds	V
Pressure vertical velocity	W
Relative humidity	RH
Geopotential height	H
Best (4-layer) index	B

5.3 Recommendations for Further Research

The results from this study showed that a linear relationship existed between averaged optical turbulence values and synoptic scale variables, but it was a weak relationship. The limited scope of this study did not permit exploration of other potential predictor variables which may strengthen the linear relationship. First, categorizing the data by vertical levels may not have been appropriate; mapping synoptic scale meteorological data to its suspected source region and using these values as potential predictors may provide better results. For example, vertical distance from the tropopause or maximum wind level and horizontal distance from jet core could be used as potential predictors. Second, a linear regression using time derivatives of specific meteorological parameters may also show a stronger relationship. Other potential predictors such as the square of a predictor or the product of one or more potential predictors could be used also. In this case, if a strong relationship was found, it would indicate a strong non-linear relationship.

In addition, a follow-on study should examine specific case studies that were available in the data sets. Since a weak relationship was found for the discontinuous period between January 1993 to January 1994, a stronger relationship may exist for certain seasons of the year. It may be advantageous to focus on a specific feature, such as the predominant predictor variables in Table 14 or the tropopause height, which migrates with season. A linear or non-linear regression for specific periods of the year may provide a stronger statistical relationship.

Although averaging optical turbulence data is common, it may not have best choice. For example, time averaging of 3-minute increments to 6 hour increments may have

68

affected the relationship by smoothing out interesting features in the C_n^2 data. No literature was found that addressed such a problem; however, a study relating C_n^2 to synoptic scale weather parameters with different time and spatial increments may provide better results.

Finally, synoptic scale variables may not fully explain the fluctuations in optical turbulence. Since optical turbulence is usually confined to thin, horizontal layers, synoptic scale variables may not be able to distinguish the fluctuations in C_n^2. Perhaps a study to determine the statistical relationship between C_n^2 and mesoscale meteorological variables may be more promising. Such a task will prove difficult, however, since data from mesoscale models is not easily accessible and may not be available in areas where the Airborne Laser will be deployed. Lastly, if the data is available, a study to determine the statistical relationship between optical turbulence and local weather phenomena can be pursued.

Bibliography

Bluestein, Howard B. Synoptic-Dynamic Meteorology in Midlatitudes, Volume II, Observations and Theory of Weather Systems. New York NY: Oxford University Press, 1993.

Cody, Ronald P. and Jeffrey K. Smith. Applied Statistics and the SAS Programming Language (Third Edition). New York NY: Elsevier Science Publishing Co., Inc., 1991.

Devore, Jay L. Probability and Statistics for the Engineering and the Sciences (Fourth Edition). Belmont CA: Duxbury Press, 1995.

Dewan, Edmond M. Optical Turbulence Forecasting: A Tutorial. Hanscom Air Force Base, MA: Air Force Geophysics Laboratory, 22 January 1980 (AFGL-TR-80-0630).

Duffield, George F. and Gregory D. Nastrom. Equations and Algorithms for Meteorological Applications in Air Weather Service. Scott Air Force Base IL: Air Weather Service, July 1984 (AWS/TR-83/001).

Frisch, A. S. and others. "The Variations of C_n^2 Between 4 and 18 km Above Sea Level as Measured Over 5 Years," Journal of Applied Meteorology, 29: 645-651 (July 1990).

General Accounting Office (GAO). Theater Missile Defense: Significant Technical Challenges Face the Airborne Laser Program. World Wide Web, http://www.gao.gov/new.items/ns98037.pdf. 23 October 1997 (GAO/NSIAD-98-37).

Haltiner, George J. and Roger Terry Williams. Numerical Prediction and Dynamic Meteorology (Second Edition). New York NY: John Wiley and Sons, Inc., 1980.

Hines, J. and others (Battlefield Environment Directorate and Science and Technology Corporation). Relative Accuracies of Wind, Virtual Temperature, and C_n^2 Profiler Measurements at the Atmospheric Profiler Research Facility, White Sands Missile Range, NM. Army Research Laboratory, April 1996 (ARL-TR-1003).

Hocking, W. K. "Measurement of Turbulent Energy Dissipation Rates in the Middle Atmosphere by Radar Techniques: A Review," Radio Science, 20: 1403-1422 (November-December 1985).

Holton, James R. An Introduction to Dynamic Meteorology (Third Edition). San Diego CA: Academic Press, Inc., 1992.

Kalney, E. and others. "The NCEP/NCAR 40-Year Reanalysis Project," Bulletin of the American Meteorological Society, 77: 437-471 (1996).

List, Robert J. Smithsonian Meteorological Tables (Sixth Edition). Washington DC: Smithsonian University Press, 1951.

Nastrom, G. D. and F. D. Eaton. "Onset of the Summer Monsoon Over White Sands Missile Range, New Mexico, as Seen by VHF Radar," Journal of Geophysical Research, 98: 23235-23243 (December 1993).

----- and -----. "The Coupling of Gravity Waves and Turbulence at White Sands, New Mexico, from VHF Radar Observations," Journal of Applied Meteorology, 32: 81-87 (January 1993).

----- and -----. "Variations of Winds and Turbulence Seen by the 50-MHz Radar at White Sands Missile Range, New Mexico," Journal of Applied Meteorology, 34: 2135-2148 (October 1995).

----- and others. "Variability of Turbulence, 4-20 km, in Colorado and Alaska from MST Radar Observations," Journal of Geophysical Research, 91: 6722-6734 (May 1986).

Ottersen, Hans. "Atmospheric Structure and Radar Backscattering in Clear Air," Radio Science, 4: 1179-1193 (December 1969).

Rinehart, Ronald E. Radar for Meteorologists (Second Edition). Grand Forks ND: Knight Printing Company, 1991.

Stull, Roland B. An Introduction to Boundary Layer Meteorology. Dordrecht, Netherlands: Kluwer Academic Publishers, 1988.

Tabachnick, Barbara G. and Linda S. Fidell. Using Multivariate Statistics. New York NY: Harper & Row, 1983.

Tatarski, V. I. Wave Propagation in a Turbulent Medium. New York NY: McGraw-Hill Book Company, 1961.

Tsuda, T. and others. "Simultaneous Observations of Reflection Echoes and Refractive Index Gradient in the Troposphere and Lower Stratosphere," Radio Science, 23: 655-665 (July-August 1988).

VanZandt, T. E. and others. "Vertical Profiles of Refractivity Turbulence Structure Constant: Comparison of Observations by the Sunset Radar with a New Theoretical Model," Radio Science, 13: 819-829 (September-October 1978).

Wallace, John M. and Peter V. Hobbs. Atmospheric Science: An Introductory Survey. San Diego CA: Academic Press, Inc., 1977.

Warnock, J. M and others. "A Statistical Model to Estimate Mean Values of Parameters of Turbulence in the Free Atmosphere," Preprints, AMS Seventh Symposium on Turbulence and Diffusion, Nov 12-15, 1985, Boulder, CO. 156-159. Boston MA: American Meteorological Society, 1986.

----- and T. E. VanZandt. A Statistical Model to Estimate the Refractivity Turbulence Structure Constant C_n^2 in the Free Atmosphere. Boulder CO: NOAA, Aeronomy Laboratory, November 1985 (NOAA TM-ERL-AL-10).

Weber, B. L. and D. B. Wuertz. Quality control algorithm for profiler measurements of winds and temperatures. October 1991 (NOAA TM-ERL-WPL-212).

Wilks, Daniel S. Statistical Methods in the Atmospheric Sciences. New York NY: Academic Press, Inc., 1995.

Vita

Capt Diana Lynn Hajek was born on 2 October 1970 in El Paso, Texas. She graduated from Irvin High School in 1988 and entered undergraduate studies at the University of Texas at El Paso. She graduated with a Bachelor of Science degree in Physics and was commissioned through the Air Force Reserve Officer Training Corps in July 1992.

Her first assignment was at Brooks AFB, Texas as a program manager for the Aeromedical Systems Division, Human Systems Center Program Office. In May 1996, she entered the school of Engineering Physics, Air Force Institute of Technology and cross-trained into the meteorology career field.

Captain Hajek is married to Emanuel Vincent Hajek III of El Paso, Texas.

Permanent Address: 3633 Wickham Avenue
El Paso, Texas 79904

REPORT DOCUMENTATION PAGE

Public reporting burden for this collection of information is estimated to average 1 hour per response, including the time for reviewing instructions, searching existing data sources, gathering and maintaining the data needed, and completing and reviewing the collection of information. Send comments regarding this burden estimate or any other aspect of this collection of information, including suggestions for reducing this burden, to Washington Headquarters Services, Directorate for Information Operations and Reports, 1215 Jefferson Davis Highway, Suite 1204, Arlington, VA 22202-4302, and to the Office of Management and Budget, Paperwork Reduction Project (0704-0188), Washington, DC 20503.

1. AGENCY USE ONLY (Leave blank)	2. REPORT DATE	3. REPORT TYPE AND DATES COVERED
	March 1998	Master's Thesis

4. TITLE AND SUBTITLE
REGRESSION ANALYSIS OF RADAR MEASURED OPTICAL TURBULENCE WITH SYNOPTIC SCALE METEOROLOGICAL VARIABLES

5. FUNDING NUMBERS

6. AUTHOR(S)
Diana L. Hajek, Capt, USAF

7. PERFORMING ORGANIZATION NAME(S) AND ADDRESS(ES)
Air Force Institute of Technology
Advisor: Lt Col Cecilia Askue (DSN 785-3636 x4642, caskue@afit.af.mil))
2750 P Street
WPAFB OH 45433-7765

8. PERFORMING ORGANIZATION REPORT NUMBER

AFIT/GM/ENP/98M-03

9. SPONSORING/MONITORING AGENCY NAME(S) AND ADDRESS(ES)
Air Force Research Laboratory (AFRL/DES)
Major Michael Johnson (DSN 246-4722, johnsonm@smtpgw1.plk.af.mil)
3550 Aberdeen Ave SE
Kirtland AFB NM 87118

10. SPONSORING/MONITORING AGENCY REPORT NUMBER

11. SUPPLEMENTARY NOTES

12a. DISTRIBUTION AVAILABILITY STATEMENT
Approved for public release; distribution unlimited

12b. DISTRIBUTION CODE

13. ABSTRACT (Maximum 200 words)

A key issue to the USAF's Airborne Laser (ABL) program is the ability to accurately predict the level of optical turbulence that the ABL will encounter at its flight levels. The optical turbulence must be characterized so that the range and range variation of the ABL can be determined. Gravity wave spectra resulting from frontal or jet stream passage are presumed to cause layers of optical turbulence; however, exact relationships between optical turbulence and synoptic scale meteorological phenomena are unclear. This study assesses the statistical relationship between optical turbulence and synoptic scale variables through multiple linear regression. The optical turbulence measurements were observed by the 50 MHz radar at White Sands Missile Range, New Mexico from January 1993 to January 1994. Measurements were averaged temporally and vertically to coincide with weather data. The synoptic scale meteorological data was extracted from the NCEP/NCAR reanalysis database. Results from the regression models showed that a linear relationship exists between optical turbulence and major synoptic scale variables; however, this relationship was a weak one. It was concluded that further research was needed to define the exact relationship between synoptic scale meteorological variables and optical turbulence.

14. SUBJECT TERMS
atmospheric refraction;atmospheric refractive index;meteorological phenomena refraction;regression analysis;electromagnetic wave propagation

15. NUMBER OF PAGES
86

16. PRICE CODE

17. SECURITY CLASSIFICATION OF REPORT	18. SECURITY CLASSIFICATION OF THIS PAGE	19. SECURITY CLASSIFICATION OF ABSTRACT	20. LIMITATION OF ABSTRACT
Unclassified	Unclassified	Unclassified	UL